Strangeness Production in the HSD Transport Approach from SIS to SPS energies*

J. Geiss†, W. Cassing and C. Greiner
Institut für Theoretische Physik, Universität Giessen
D-35392 Giessen, Germany

Abstract

We study systematically the production of strangeness in nuclear reactions from SIS to SPS energies within the covariant hadronic transport approach HSD. Whereas the proton and pion rapidity distributions as well as pion transverse momentum spectra are well described in the hadronic transport model from 2-200 A·GeV, the K^+ and K^- spectra are noticeably underestimated at AGS energies while the K^+ spectra match well at SIS and SPS energies with the experimental data. We conclude that the failure of the hadronic model at AGS energies points towards a nonhadronic phase during the collision of heavy systems around 10 A·GeV.

1 Introduction

The aim of high energy heavy-ion collisions especially at the Brookhaven Alternating Gradient Synchrotron (AGS) and the CERN Super Proton Sychrotron (SPS) is to investigate nuclear matter under extreme conditions, i.e. high temperature and high density. The most exciting prospect is the possible observation of a signal for a phase transition from normal nuclear matter to a nonhadronic phase, where partons are the basic degrees of freedom. In this context Rafelski has introduced strangeness enhancement in heavy-ion collisions compared to proton-proton collisions as a possible signature for the phase transition [1]. Especially the abundancies of multistrange baryons and strange antibaryons should be increased drastically. The idea is based on a different production mechanism of strangeness in a partonic and hadronic phase, respectively. In the partonic phase the mass of the strange quark is of the order of the temperature resulting in a rapid chemical equilibration of the flavors, u d and s, if the partonic phase is of sufficient size and duration to form an equilibrated quark-gluon plasma (QGP). The timescale for chemical equilibration in a QGP is estimated to be of the order $2-3$ fm/c [2, 3, 4]. In contrast, the equilibration time of strange hadrons in

*Supported by BMBF and GSI Darmstadt
†Part of the PhD thesis of J. Geiss

a pure thermally equilibrated hadronic phase is expected to be an order of magnitude larger [2], because the threshold for strange hadron production is large compared to typical temperatures expected in a heavy-ion collision at AGS or SPS energies.

Indeed it has been found experimentally, that the strange hadron yields normalized to the pion abundancies are enhanced in A + A collisions at AGS and SPS energies [5]. In particular a strong increase of the production of strange antibaryons and multistrange baryon/antibaryons has been observed experimentally. Nevertheless, there is still a theoretical debate, if the observed strangeness enhancement is a clear signature for a QGP. Detailed calculations of the production mechanism are difficult due the nonperturbative nature of the hadronization process and phenomenological models must be introduced to describe hadron condensation.

Several microscopic approaches have been used to describe ultrarelativistic heavy-ion collisions. Most of them describe the early prehadronic phase and hadronization in terms of the string picture for the high energy hadronic interactions such as the HSD approach [6]. Other popular models of this type are FRITIOF [7] or the recently extended version LUCIAE [8], VENUS [9], RQMD [10], DPM [11], QGSM [12], ARC [13], ART [14] and UrQMD [15]. The strings, representing a prehadronic stage, are characterized by the constituent incomming quarks and a tube of color flux is supposed to be spanned in between. While in HSD, FRITIOF and UrQMD the strings are assumed to hadronize independently, recent RQMD versions and VENUS versions include some kind of string fusion resulting in color ropes [16, 17] or quark droplets [18], which may be seen as a 'mini-QGP', to achieve a better agreement with data, especially the strange baryon-antibaryon yield, at SPS energies. In the RQMD model, for example, the color rope then fragments in a collective way and tends to enhance the production of strange quark pairs and especially of diquark-antidiquark pairs [19]. The production of strange baryon-antibaryon pairs is enhanced drastically by this collective effect while the enhancement of the total strangeness yield, mainly kaons, at SPS energies was found to be dominated by hadronic rescattering and not by an increasing $s\bar{s}$ yield at the hadronization process. In a similar way Tai An and Sa Ben-Hao describe the enhancement of strange antibaryons and multistrange baryons at SPS energies within LUCIAE, which is based on the FRITIOF model and includes hadronic rescattering and some collective string interaction [8]. This collective interaction tends to enhance the probability for strangeness and diquark production during the string fragmentation process as a function of centrality and mass of the system [8]. In the present work the strangeness production in proton-nucleus and heavy-ion collisions is investigated within a dynamical hadronic description, the HSD approach [6]. No enhancement of the primary strangeness production during the hadronization phase is included as well as no kind of string-string interaction.

Another class of models are the parton models HIJING [20], HIJET [21] and VNI [22], which are based on the concept that the colliding nuclei can be decomposed into their parton substructure. The parton models include cross sections from perturbative QCD requireing high momentum transfers $q^2 > 10$ GeV^2 in parton scatterings. At SPS energies this may be fullfilled for the first collisions, but most of the reactions are supposed to be softer and require a nonperturbative treatment. For that reason the application of parton models at SPS energies remains questionable; the situation will

become better at RHIC and LHC energies.

In contrast to microscopic models also (global) thermal models have been employed due to their simplicity [23, 24, 25, 26]. Here the hot and dense system is assumed to be in local thermal and chemical equilibrium at the time of freeze-out. Thermal models state nothing about the history of the fireball, if it was created by a pure hadronic system or a QGP. Thus there is a total 'memory loss'. Nevertheless, thermal models are attractive, because they predict all particle abundancies in terms of only three parameters, the temperature T, the baryochemical potential μ_B and the volume of the fireball V_f. Absolute particle number ratios reflect the thermal and chemical conditions at freezout, while the spectra of particles combine thermal motion and collective flow. A lot of data at AGS and SPS energies has been found to be consistent with thermal models within a factor of 2 [23]. For the strangeness production a new incomplete strangeness saturation parameter has to be included [24] in order to refine the agreement.

On the other hand, many of the dynamical microscopic models are not designed to work over a broad energy range. The VENUS model is fine tuned to SPS energies and ARC is presently only designed for AGS energies. An extention to higher energies including hard processes as described in [27] will increase the applicability of ARC in future. The parton models on the other hand are restricted to very high energies as mentioned above. On the other hand a systematic study over a wide energy range (SIS-SPS) from light to heavy systems is of particular interest for the topic of strangeness enhancement in heavy-ion collisions, because recent data from AGS and SPS show that the scaled strangeness yield (K/π) seems to be essentially higher at AGS energies. Such a systematic investigation can presently only be performed within the HSD, RQMD or UrQMD models. Within the RQMD model there exist calculations for strangeness production at AGS [28] and at SPS energies [16, 19, 29], but these investigations are performed within different RQMD versions.

The aim of the present work is to perform a systematic analysis of strangeness production within the HSD approach and to present the elementary strangeness production channels. Recently a lot of data for the most heavy systems has been published [5]; thus it is possible to compare our results to the data for many systems from SIS to SPS energies within one fixed version of the transport code.

Our work is organized as follows: In Section 2 we will give a brief description of the HSD approach. The primary elementary hadron-hadron collisions are described in detail and the dynamics of the strings in heavy-ion collisions as well as the formation time concept is presented. The particle production and stopping of incoming hadrons for elementary baryon-baryon collisions is investigated over a wide energy range. We then extend our study to the strangeness production from string fragmentation and from rescattering processes. We compare our results with data from proton-proton and pion-proton collisions from the threshold up to 100 GeV. In Section 3 we test the global dynamics from AGS to SPS energies obtained in the HSD model for different systems. We compare our results for stopping and particle production to data and show that the global dynamics is reasonably well described within the HSD approach, which also was found at SIS energies before [30, 31]. In Section 4 we show our results for strangeness production in heavy-ion collisions at AGS and SPS energies in comparison with the

available data. In Section 5 we present the results of our calculation for pion and kaon spectra from 2 to 11 A·GeV thus providing a link between SIS and AGS energies. In Section 6, finally, we give a summary and discussion of open problems.

2 The covariant transport approach

In this work the dynamical analysis of p + p, p + A and A + A reactions is performed within the HSD approach [6] in the cascade modus which is based on a coupled set of covariant transport equations for the phase-space distributions $f_h(x,p)$ of hadron h [6], i.e.

$$\left(\frac{\partial}{\partial t} + \frac{\vec{p}_1}{m}\vec{\nabla}\right) f_1(x,p_1) = \sum_{2,3,4\ldots} \int d2d3d4 \ldots [G^\dagger G]_{12\to 34\ldots} \delta^4(p_1^\mu + p_2^\mu - p_3^\mu - p_4^\mu \ldots) \times \Big\{ f_3(x,p_3) f_4(x,p_4) \bar{f}_1(x,p) \bar{f}_2(x,p_2) - f_1(x,p) f_2(x,p_2) \bar{f}_3(x,p_3) \bar{f}_4(x,p_4) \Big\} \ldots \quad . \tag{1}$$

Here $[G^\dagger G]_{12\to 34\ldots}\delta^4(p_1^\mu + p_2^\mu - p_3^\mu - p_4^\mu \ldots)$ is the 'transition rate' for the process $1+2 \to 3+4+\ldots$, while the phase-space factors

$$\bar{f}_h(x,p) = 1 \pm f_h(x,p) \tag{2}$$

are responsible for fermion Pauli-blocking or Bose enhancement, respectively, depending on the type of hadron in the final/initial channel. The dots in eq. (1) stand for further contributions in the collision term with more than two hadrons in the final channels. We note that collisions with more than two hadrons in the initial channel are not included due to technical reasons.

The transport approach (1) is fully specified by the transition rates $G^\dagger G\, \delta^4(\ldots)$ in the collision term, that describes the scattering and hadron production and absorption rates. In the cms of the colliding particle the transition rate is given by

$$G^\dagger G\, \delta^4(\ldots) = v_{12}\, \left.\frac{d\sigma}{d\Omega}\right|_{1+2\to 3+4+\ldots} , \tag{3}$$

where $d\sigma/d\Omega$ is the differential cross section of the reaction and v_{12} the relative velocity of particles 1 and 2. The HSD transport approach was found to describe reasonably well hadronic as well as dilepton data from SIS to SPS energies [6, 30, 31, 32].

In the present version we propagate explicitly baryons (p, n, Δ, N(1440), N(1535), Λ, Σ, Σ^*, Ξ, Ω), the corresponding antibaryons and mesons (pions, kaons, η's, η''s, ρ, ω, ϕ, K^*, a_1). The baryon-baryon collisions are described using the explicit cross sections as in the BUU model [33] for invariant energies $\sqrt{s} < 2.65$ GeV, which have been successfully tested in the energy regime below 2 A·GeV bombarding energy - and by the FRITIOF model [7] (for $\sqrt{s} > 2.65$ GeV). For meson-baryon reactions the same

concept is used, where a transition energy of 2.1 GeV is employed. In the BUU model [33] the following reaction channels are included

$$\begin{aligned} NN &\leftrightarrow N'N' \\ NN &\leftrightarrow NR \\ NR &\leftrightarrow N'R' \\ \Delta\Delta &\leftrightarrow N'R' \\ R &\leftrightarrow N\pi \\ N(1535) &\leftrightarrow N\eta \\ NN &\leftrightarrow NN\pi, \end{aligned} \tag{4}$$

where R stands for a resonance $\Delta, N(1440)$ or $N(1535)$. Additionally the channels

$$\begin{aligned} \rho N &\rightarrow N\pi\pi \\ \omega N &\rightarrow N\pi\pi\pi \end{aligned} \tag{5}$$

are included with an energy independent cross section of 30 mb.

The measured total and elastic baryon-baryon (p + p, p + n) and meson-baryon (π^+ + p, π^- + p, K^- + p, K^+ + p) cross sections are to a good approximation independent of the incoming isospins for energies above the string threshold. Paramerizations of the experimental p + p, p + n, π^+ + p, π^- + p, K^- + p, K^+ + p cross sections are taken from Ref. [34]. The cross sections for the other hadron-hadron channels must be specified in the transport model for collision energies above the string threshold ($\sqrt{s} =$ 2.65 GeV for baryon-baryon, $\sqrt{s} = 2.1$ GeV for meson-baryon); in the HSD approach these high energy cross sections are related to the measured cross sections by

$$\begin{aligned} \sigma_{tot}^{N\Delta}(\sqrt{s}) &= 0.5\left(\sigma_{tot}^{pp}(\sqrt{s}) + \sigma_{tot}^{pn}(\sqrt{s})\right) \\ \sigma_{tot}^{\rho N}(\sqrt{s}) = \sigma_{tot}^{\rho\Delta}(\sqrt{s}) &= \sigma_{tot}^{\omega\Delta}(\sqrt{s}) = \ldots \\ &= 0.5\left(\sigma_{tot}^{\pi^+ N}(\sqrt{s}) + \sigma_{tot}^{\pi^- N}(\sqrt{s})\right) \\ \sigma_{tot}^{KN}(\sqrt{s}) = \sigma_{tot}^{K\Delta}(\sqrt{s}) &= \ldots = \sigma_{tot}^{K^+ p}(\sqrt{s}) \\ \sigma_{tot}^{\bar{K}N}(\sqrt{s}) = \sigma_{tot}^{\bar{K}\Delta}(\sqrt{s}) &= \ldots = \sigma_{tot}^{K^- p}(\sqrt{s}). \end{aligned} \tag{6}$$

The dots in Eq.(4) stand for all other combinations in the incoming chanels. The same procedure is applied for the elastic cross sections. The high energy inelastic baryon-baryon (meson-baryon) cross sections obtained by this procedure are ≈ 30 (20) mb, which correspond to the typical baryonic (mesonic) geometrical cross sections, i.e. $\sigma^{inel} \approx \pi R^2$. In ultrarelativistic heavy-ion collisions with a lot of rescattering processes this should be a reasonable and conservative input for the calculation.

In order to be consistent with the experimental inelastic pion-proton cross section below the string threshold, an additional channel besides the cross section from the BUU model [33] is included: $\pi N \rightarrow \pi\pi N$. This reaction fills up the inelastic cross section and ensures a smooth transition at the string threshold as shown in Fig. 1

(upper part), where the calculated total and elastic $\pi^+ p$ cross section together with the experimental data [34] are shown. The low energy nucleon-nucleon cross sections taken from the BUU model fit reasonable well to the high energy parametrizations as shown in Fig. 1 (lower part) together with the data from [34].

At ultrarelativistic (SPS) energies meson-meson reactions may become even more important, because the intermediate meson density is much higher than the baryon density. However, the average invariant energy of these secondary or higher order reactions is rather small. It is thus convenient to use cross sections within the Breit-Wigner resonance picture adopting branching ratios from the nuclear data tables [34] without introducing new parameters. The reactions of the type $a + b \rightarrow m_R \rightarrow c + d$, where a,b,c and d denote the mesons in the initial and final state and m_R the mesonic intermediate resonance (ρ, a_1, ϕ, K^*), is described by the cross section

$$\sigma(ab \rightarrow cd) = \frac{2J_R + 1}{(2S_a + 1)(2S_b + 1)} \cdot \frac{4\pi}{p_i^2} \cdot \frac{s\Gamma_{R\rightarrow ab}\Gamma_{R\rightarrow cd}}{(s - M_R^2)^2 + s\Gamma_{tot}^2}. \tag{7}$$

In Eq.(7) S_a, S_b and J_R are the spins of the particles; $\Gamma_{R\rightarrow ab}$ and $\Gamma_{R\rightarrow cd}$ denote the partial decay width in the initial and final channels, M_r and Γ_{tot} the mass and the total resonance width and p_i is the initial momentum in the resonance rest frame. The following meson-meson reactions are included:

$$\pi\pi \leftrightarrow \rho, \quad \pi\rho \leftrightarrow \phi, \quad \pi\rho \leftrightarrow a1, \quad \pi K \leftrightarrow K^*. \tag{8}$$

Additionally strangeness production by meson-meson collision is included, which is expected to contribute at AGS and SPS energies, where a high mesonic density is achieved. An isospin averaged cross section [30]

$$\bar{\sigma}_{mm\rightarrow K\bar{K}}(s) = 2.7 \cdot \left(1 - \frac{s_0}{s}\right)^{0.76} \text{[mb]}, \quad s_0 = 4m_K^2 \tag{9}$$

is applied, where mm stand for all possible nonstrange mesons in the incoming channel, e.g.

$$\pi\pi \rightarrow K\bar{K}, \quad \pi\rho \rightarrow K\bar{K}, \quad \ldots. \tag{10}$$

2.1 Elementary baryon-baryon collisions

The primary elementary inelastic collisions of hadron pairs are the essential input for the microscopic simulation of heavy-ion collisions. For the present analysis the elementary strangeness production in pp collisions over a wide energy range is of particular interest and serves as a reference for strangeness enhancement in heavy-ion collisions.

In the HSD approach the high energy inelastic hadron-hadron collisions are described by the FRITIOF model [7], where two incoming hadrons will emerge the reaction as two excited color singlet states, i.e. strings. The energy and momentum transfer in the FRITIOF model are assumed to happen instantanously at the collision time. With this phenomenological description of the soft processes the global properties of heavy-ion collisions can be described very well (see section 3). Observables which are

sensitive to hard parton-parton processes, like e.g. Drell-Yan production or pion production with highest Feynman x, cannot be described within this approach [35] (for a detailed discussion of this topic see [27]). However, the observables discussed in the present paper in the energy range 2-200 A·GeV, i.e. low to moderate transverse momentum particle production, are dominated by the soft processes, which are described by string excitation and fragmentation.

According to the Lund string model [36] a string is characterized by the leading constituent quarks of the incoming hadron and a tube of color flux is supposed to be formed connecting the rapidly receding string-ends. In the HSD approach baryonic $(qq-q)$ and mesonic $(q-\bar{q})$ strings are considered. In the uniform color field of the strings virtual $q\bar{q}$ or $qq\bar{q}\bar{q}$ pairs are produced causing the tube to fission and thus create mesons or baryon-antibaryon pairs. The production probability P of massive $s\bar{s}$ or $qq\bar{q}\bar{q}$ pairs is suppressed in comparison to light flavor production ($u\bar{u}$, $d\bar{d}$) according to a Schwinger-like formula [37]

$$\frac{P(s\bar{s})}{P(u\bar{u})} = \gamma_s = exp\left(-\pi\frac{m_s^2 - m_q^2}{2\kappa},\right) \tag{11}$$

with $\kappa \approx 1GeV/fm$ denoting the string tension. Thus in the Lund string picture the production of strangeness and baryon-antibaryon pairs is controlled by the constituent quark and diquark masses. Inserting the constituent quark masses $m_u = 0.3$ GeV and $m_s = 0.5$ GeV a value of $\gamma_s \approx 0.3$ is obtained. While the strangeness production in proton-proton collisions at SPS energies is reasonably well reproduced with this value, the strangeness yield for p + Be collisions at AGS energies is underestimated by roughly 30%, as we will show in the next section. For that reason the suppression factors used in the HSD model are

$$u:d:s:uu = \begin{cases} 1:1:0.3:0.07 & \text{, at SPS energies} \\ 1:1:0.4:0.07 & \text{, at AGS energies,} \end{cases} \tag{12}$$

with a linear transition of the strangeness suppression factor as a function of $\sqrt{s}$ in between.

The production probability for $qq\bar{q}\bar{q}$ pairs in the HSD model is reduced to

$$\frac{P(qq\bar{q}\bar{q})}{P(u\bar{u})} = 0.07 \tag{13}$$

compared to the standart FRITIOF parameter 0.1 in order to get better agreement with $\bar{p}$ and $\bar{\Lambda}$ production in p + p collisions at SPS energies as we will show in the next section. This parameter has no influence on the global strangeness production in heavy-ion collisions.

Additionally a fragmentation function $f(x, m_t)$ has to be specified, which is the probability distribution for hadrons with transverse mass m_t to acquire the energy-momentum fraction x from the fragmenting string

$$f(x, m_t) \approx \frac{1}{x}(1-x)^a exp\left(-bm_t^2/x\right), \tag{14}$$

where $a = 0.23$, $b = 0.34\,GeV^{-2}$ are used in the HSD model.

In order to get some confidence about the particle production from the FRITIOF model, we show in Fig. 2 the invariant cross sections for inclusive proton (upper part) and π^+ production in proton-proton collisions at $p_{lab} = 12$ GeV in comparison to the data from Ref. [38]. The π^+ spectra are shown in the lower part for three different intervals of transverse momentum and have a Gaussian shape while the proton rapidity distribution is peaked around target and projectile rapidity (upper part). The comparison with the data indicates a slightly too high stopping obtained within the FRITIOF model at midrapidity, which one should keep in mind when analyzing stopping in heavy-ion collisions. In Fig. 3 the rapidity distributions of protons (dashed line) and negatively charged hadrons (solid line) for proton-proton collisions at SPS energies ($p_{lab} = 200$ GeV) are shown. Again a good agreement with the data is found in rapidity space for the produced particles.

The particle distribution in transverse momentum is illustrated in Fig. 4a, where we show the p_t spectra of π^+, K^+, K^-, p and $\bar{p}$ for inelastic proton-proton collisions at $\sqrt{s} = 23$ GeV (SPS energies) at midrapidity $|y| \leq 0.1$ in comparison to the data from Ref. [40]. The calculated spectra and the data at midrapidity are not exponential; the pions show a clear low-p_t and high-p_t enhancement opposite to p and $\bar{p}$ spectra. The situation is different at AGS energies as demonstrated in Fig. 4b, where the transverse momentum spectra of π^+, π^- and K_s^0 for inelastic proton-proton collisions at $p_{lab} = 12$ GeV are shown in comparison with the data from Ref. [38]. The overall agreement of particle production, both in transverse momentum and in rapidity space, obtained within the FRITIOF model from AGS to SPS energies is rather good.

The complete energy regime can be tested by data for energy dependent cross sections for the reactions $p + p \rightarrow 2\,prongs + X$, $p + p \rightarrow 4\,prongs + X$ and $p + p \rightarrow 6\,prongs + X$ (*prongs*: charged particles) as shown in Fig. 5 together with the experimental data from [41]. We note that the particle production from the FRITIOF model, which is taken in the HSD approach for inelastic baryon-baryon collisions, fits reasonably well the data from SPS energies down to the string threshold $\sqrt{s} = 2.65$ GeV.

The implementation of this string fragmentation model into a covariant transport theory implies to use a time scale for the particle production process, i. e. the formation time t_f. The formation time includes the formation of the string, the fission of the string due to $q\bar{q}$ and $qq\bar{q}\bar{q}$ production into small substrings and the time to form physical hadrons. It can be interpreted as the time needed for a hadron to tunnel out of the vacuum and to form its internal wavefunction. In the HSD model the formation time is a single fixed parameter for all hadrons and is set to $t_f = 0.8\ fm/c$ [6] in the rest frame of the new produced particle. In the center of mass of a string the hadronization starts after the formation time and proceeds to the stringends as illustrated in Fig. 6. The formation point of a new produced hadron with velocity $\vec{\beta}$ in the string cms is given by

$$\vec{x} = \vec{x}_{coll} + \vec{\beta} \cdot t_f, \tag{15}$$

where $\vec{x}_{coll}$ is the collision point of the two incoming hadrons.

Due to time dilatation and Lorentz γ-factors of $\approx 2-6$ for the leading constituent quarks for AGS to SPS energies the formation time of the leading hadrons are long in comparison to the time between two consecutive collisions in heavy-ion reactions. Thus applying the concept of string fragmentation to heavy-ion collisions one has to specify the interaction of strings and their constituents with the surrounding hadrons. Here a similar picture as in the UrQMD model [15] is used: The cross section of the secondary interactions of the leading quarks/diquarks are reduced prior to the formation as

$$\begin{aligned} \sigma(q-B) &= 1/3\,\sigma(B-B) \approx 10mb \\ \sigma(qq-B) &= 2/3\,\sigma(B-B) \approx 20mb \\ \sigma(qq-q) &= 2/9\,\sigma(B-B) \approx 6.6mb \end{aligned} \tag{16}$$

and so on. In order to treat this scheme within the FRITIOF string picture the q (qq) is assumed to form a meson (baryon) together with its prospective quark partner inside the string. This procedure has to be seen as a heuristic approximation of the underlying soft partonic dynamics. Nevertheless, the global properties of heavy-ion collisions, the baryon stopping and pion production, can be described with this procedure over a wide energy range as we will show in Section 3.

The interaction of the string field spanned between the constituent quarks with other hadrons is not taken into account. This is motivated by the fact, that most of the strings in a given space-time volume fragment within a small time intervall. Thus the interaction of secondaries with the string field should be negligible in first order. Furthermore, since most of the strings are stretched longitudinally, no string-string interaction or a string fusion to color ropes as suggested in [16, 17] is included in order to avoid new parameters.

2.2 Strangeness production in elementary hadron-hadron collisions

Of particular interest for the present analysis is the strangeness production in the elementary hadron-hadron collisions. To obtain agreement with p-p data at SPS energies and with p-Be at AGS energies the strangeness suppression factor γ_s in the FRITIOF model had to be enhanced from $\gamma_s = 0.3$ (SPS) to $\gamma_s = 0.4$ (AGS) as mentioned above. To illustrate this we show in Table 1 the particle multiplicities obtained in p-p collisions at $p_{lab} = 200$ GeV in comparison to the experimental data from [42]. The agreement in the strangeness sector is very good, however, the $\Lambda + \Sigma^0$ yield is overestimated by roughly 30%, but is fixed in the calculation by the K^+, K^- and K_s^0 yield due to strangeness conservation. At AGS energies the suppression factor γ_s=0.4 is choosen in order to describe the kaon production in p + Be collisions; otherwise the strangeness production here would be underestimated by 30% (see Fig. 13).

Since the string model is designed to describe inelastic hadron-hadron collisions at rather high energies, its results for the strangeness production down to threshold become questionable. On the other hand the low energy cross sections are of particular interest for strangeness production during the rescattering phase. For that reason explicit parametrizations of the channel $NN \to NYK$ have to be used. The isospin

particle	data	HSD
π^+	3.22 ± 0.12	3.25
π^-	2.62 ± 0.06	2.53
π^0	3.34 ± 0.24	3.36
K^+	0.28 ± 0.06	0.274
K^-	0.18 ± 0.05	0.18
K_s^0	0.17 ± 0.01	0.174
$\Lambda + \Sigma^0$	0.1 ± 0.015	0.15
$\bar{\Lambda} + \Sigma^0$	0.013 ± 0.01	0.018
p	1.34 ± 0.15	1.32
$\bar{p}$	0.05 ± 0.02	0.057

Table 1: Particle multiplicities for inelastic proton-proton collisions at $p_{lab} = 200$ GeV compared to the data from [42].

averaged cross sections of this channel are related to the measured channel as:

$$\begin{aligned} \sigma_{NN\to N\Lambda K} &= 3/2\, \sigma_{pp\to p\Lambda K^+} \\ \sigma_{NN\to N\Sigma K} &= 3/2\, \left(\sigma_{pp\to p\Sigma^+ K^0} + \sigma_{pp\to p\Sigma^0 K^+}\right). \end{aligned} \tag{17}$$

The explicit cross sections are approximated by a fit to experimental data and are specified in Ref. [30]. The same procedure is applied to other combinations of incoming particles (p, n, Δ), where isospin averaged cross section for the low energy parametrisations are taken (for details see Ref. [30]).

The total kaon production in p + p collisions from threshold up to $\sqrt{s} = 100$ GeV within the HSD approach is presented in Fig. 7a as a function of the invariant energy above threshold $\sqrt{s} - \sqrt{s_0}$ together with the experimental data [41, 43, 44, 45]. In the HSD approach the K^- are produced in baryon-baryon collisions only via string fragmentation, because the threshold $\sqrt{s_0} = 2 \cdot m_p + 2 \cdot m_k$ is above the string threshold. On the other hand the threshold for K^+ production $\sqrt{s_0} = m_p + m_\Lambda + m_K = 2.55$ GeV is below the string threshold as shown in Fig. 7a. The low energy parametrization of the kaon production (c.f. eq. (17)), which is also shown in Fig. 7a, gives a smooth transition at the string threshold. Thus the kaon production in nucleon-nucleon collisions can be reproduced within the HSD approach over many orders of magnitude.

A further important strangeness production channel are meson-baryon collisions, which are especially important in heavy systems where the secondary mesons are produced after the formation time $\gamma \times t_f$ inside the nuclei. The same procedure as for baryon-baryon collisions is applied below the string threshold (2.1 GeV). For the channels

$$\begin{aligned} \pi N &\to YK \\ \pi\Delta &\to YK, \end{aligned} \tag{18}$$

where $Y = \Lambda, \Sigma$ and $K = K^+, K^0$, we adopt the detailed parametrizations from Tsushima et al. [46]. The reaction $\pi N \to NK\bar{K}$ is also included with a cross section

taken from Ref. [30]

$$\sigma(\pi^- p \to p K^0 K^-) = 1.121 \left(1 - \frac{s_0}{s}\right)^{1.86} \left(\frac{s_0}{s}\right)^2 [mb] \tag{19}$$

where $\sqrt{s_0} = m_N + 2m_K$, which is a parametrization of the experimental data. Using isospin symmetries [30] the different isospin channels are related to $\sigma(\pi^- p \to p K^0 K^-)$.

For $\sqrt{s} > 2.1$ GeV strangeness is only produced by string fragmentation. However, the strangeness production in meson-baryon collisions calculated with the FRITIOF model underestimates the experimental data in this energy regime by $\approx 1mb$ as shown in Fig. 7b, where the dashed line is the FRITIOF result for the inclusive cross section $\pi^- p \to strangeness + X$. This difference can easily be understood within the FRITIOF string picture: The remnants of a hadron-hadron collision are always two strings and the number of incoming constituent quarks remains unchanged. Thus strangeness production in this string picture is always connected with new particle production. For baryon-baryon collisions this is reasonable, while for meson-baryon collisions it is no longer valid because a reaction like $\pi N \to K\Lambda$ never can be described. This corresponds to an annihilation of constituent quarks $u\bar{u} \to s\bar{s}$, which is not included in the FRITIOF model. For that reason we add the channel $\pi N \to K\Lambda$ explicitly with an energy independent cross section of 1 mb resulting in a better description of strangeness production in πN collision. In Fig. 7b the HSD result for the inclusive cross section $\pi^- p \to strangeness + X$ is shown by the solid line in comparison to the data [41].

3 Baryon stopping and pion production

Since the baryon and pion dynamics of nucleus-nucleus collisions at SIS energies has been investigated in detail in Refs. [6, 30, 31] we focus on AGS and SPS energies in this Section.

3.1 AGS energies

At AGS energies ($\leq$ 15 A·GeV) the initial nucleon-nucleon collisions occur at $\sqrt{s} \approx$ 5 GeV and the Lorentz contraction of the nuclear density in the nucleon-nucleon cms amounts to $\gamma_{cm} \approx 3$. Thus most of the mesons produced in p + Be reactions hadronize (after their formation time $t_f \times \gamma$) in the vacuum without rescattering such that this light system may serve as a test for the LUND string-model employed at $\sqrt{s} \approx 5$ GeV. In this respect we show in Fig. 8 the inclusive proton and π^- rapidity spectra for p + Be and p + Au at 14.6 A·GeV in comparison to the data from the E802 Collaboration [47]. The approximate symmetry of the π^- rapidity distribution around midrapidity y_{CM} for p + Be indicates very little rescattering of the pions. Also the proton distribution is rather well reproduced by the calculation for $t_f = 0.8$ fm/c, which we consider as the 'default' value for the universal formation time.

The effect of pion rescattering on nucleons and secondary pion production channels in p + Au at 14.6 GeV collisions can be extracted from the lower part of Fig. 8 where the

pion rapidity distribution is no longer symmetric around y_{CM}, but sizeably enhanced at target rapidity ($y_{lab} \approx 0$). The stopping of protons (dashed line) is also clearly visible in the proton rapidity distribution, both in the calculations as well as in the data of the E802 Collaboration [47].

The next system addressed is Si + Al at 14.6 A·GeV. The computed rapidity distribution of protons and π^--mesons for central collisions (b $\leq$ 1.5 fm) is compared in Fig. 9a to the data from Ref. [48]. Whereas the proton rapidity distribution turns out to be quite flat in rapidity y due to proton rescattering, the pion rapidity distribution is essentially of Gaussian shape which reflects the pion rapidity spectrum from the string fragmentation model (cf. Fig. 2). We note, however, that the width of the pion rapidity distributions in the HSD approach is wider compared to the E802 data. In the calculation the full width at half maximum (FWHM) ($\approx$ 2.8) is only tiny lowered compared to p + p collisions ($\approx$ 2.9, c.f. Fig. 2) due to the small amount of rescattering in Si + Al. The maxima in the calculated rapidity spectra at target and projectile rapidity do not show up in the data due to acceptance cuts.

In analogy to Fig. 4 we show in Fig. 10 the calculated transverse mass-spectra of π^--mesons for Si + Al at 14.6 A·GeV (solid lines) in comparison to the experimental data from Ref. [48]. The overall agreement for rapidities of $y_{lab} = 0.5, 0.7, 0.9, 1.1, 1.3$ seems to indicate that the general reaction dynamics for pions is rather well reproduced within the HSD approach, although the π^- rapidity spectrum is slightly narrower in experiment as compared to the calculations.

Nucleon stopping becomes more pronounced for the system Si + Au at 14.6 A·GeV as seen from Fig. 9b where the calculated proton and π^- rapidity distributions (for $b \leq 3.5$ fm) are compared to the data from E802 [48] (full squares). Whereas the proton stopping is reasonably well reproduced by the calculation the pion spectra again clearly come out too broad in rapidity as compared to the experimental data. The overestimate of pions in the HSD approach in Si + Au collision is in agreement with the findings within the RQMD model [28] and the ARC model [13]. Thus the experimentally observed strong reduction in the width of the pion rapidity spectra in heavy-ion collisions compared to p + p collisions at AGS energies, already observed in the light system Si + Al, seems to be a general problem for microscopic hadronic models.

The amount of stopping at AGS energies is most clearly pronounced for central Au + Au reactions as displayed in Fig. 9c for the proton and π^- rapidity distributions in comparison to the experimental data from Refs. [49, 50]. Though the pion rapidity spectrum - which again comes out slightly too broad in the calculation - does not differ very much in shape from that of the Si + Al system in Fig. 9a at first sight, the baryon distribution in momentum space for Si + Al is far from kinetic equilibrium whereas that for Au+Au at 11 A·GeV shows a clear approach versus equilibration (cf. [6]). We note that the proton rapidity spectrum for central Au + Au collisions at this energy shows a similar amount of stopping as the RQMD approach [16], the ART calculations by Li and Ko [14] or the ARC calculations by Kahana et al. [13].

3.2 SPS energies

We continue our comparison to experimental data with the system S + S at 200 A·GeV, i.e. the SPS regime. In Fig. 11 (l.h.s.) we show the proton and negatively charged hadron (essentially π^-) rapidity distributions in comparison to the experimental data from [51]. Though the experimental proton and h^- rapidity spectra are approximately reproduced, we cannot conclude on the general applicability of our approach at SPS energies, because also more simple models like HIJING or VENUS – with a less amount of rescattering – can reproduce the data in a similar way [52, 53]. This is due to the fact that at 200 A·GeV the Lorentz contraction in the cms amounts to $\gamma_{cm} \approx 10$ such that hadronization essentially occurs in the vacuum again and rather *little* rescattering occurs in S + S collisions. We note that the width of the pion rapidity spectrum in S + S ($\approx$ 3.8) is comparable to p + p collisions (c.f. Fig. 3) in contrast to the experimental findings at AGS energies as mentioned in the previous Section.

The transverse momentum spectra of negatively charged hadrons for central S + S reactions at 200 A·GeV are shown in Fig. 12 in comparison to the data in the cm rapidity interval $0.8 \leq y \leq 2.0$ and $2.0 \leq y \leq 3.0$ from [51]. The agreement between the data and the HSD calculations is sufficiently good such that the baryon and pion dynamics for the system S + S is reasonably well under control.

The next system of our considerations are central S + Au reactions at 200 A·GeV. In Fig. 11 (middle) the π^- and proton rapidity distributions in comparison to the data from [54, 55] are shown. Here the proton rapidity spectrum shows a narrow peak at target rapidity ($y_{CM} \approx$ -3.03) which is easily attributed to the spectators from the Au target. The bump at $y_{CM} \approx$ -2 is mainly due to rescattering of target nucleons. Note that there is no longer any yield at projectile rapidity ($y \approx 3.03$) which implies that all nucleons from the projectile have undergone inelastic scatterings. Furthermore, around midrapidity the π^- distribution is large compared to the proton distribution.

Baryon stopping is most clearly seen for the system Pb + Pb at 160 A·GeV. In Fig. 11 (r.h.s) we show the proton and h^- rapidity distributions in comparison to the data from NA49 [56]. Our computed proton rapidity spectrum for central collisions ($b \leq 2.5$ fm) is rather flat at midrapidity. It shows no dip as the HIJING [52] or VENUS [53] simulations , and is not peaked at midrapidity as compared to RQMD simulations [16]. Thus full stopping is not achieved at SPS energies even for this heavy system. On the other hand, the h^- rapidity distributions are very similar to the S + S case, however, enhanced by about a factor of $6.5 \approx 208/32$.

Summarizing this Section, the proton and pion rapidity distributions and transverse pion spectra look reasonably well for the systems studied experimentally at AGS and SPS energies. Nevertheless, we note that the HSD pion rapidity spectra at AGS energies are slightly too broad compared to data. The width of the pion spectra for heavy-ion collisions calculated within the HSD model is only slightly decreased compared to p + p collisions due to rescattering. The calculated FWHM of rapidity spectra at AGS energies changes form 2.9 (p + p) over 2.8 (Si + Al) to 2.6 (Au + Au) and for SPS energies from 3.9 (p + p) over 3.8 (S + S) to 3.8 (Pb + Pb) as expected within an independent string scenario, while experimentally a stronger decrease is observed at AGS energies.

4 Strangeness production

4.1 AGS energies

Previous investigations of strangeness production up to 2 A·GeV within the HSD model [30, 31] have given evidence especially for antikaon potentials in the medium due to the strong increase of the elementary production cross section with the excess energy $\sqrt{s}-\sqrt{s}_{thres}$ [30]. While the antikaon yield was enhanced considerably by the potentials, the kaon abundancies were found to be affected only slightly due to a small repulsive kaon potential.

Here we extend the investigations about strangeness production to AGS energies (10 - 15 A·GeV), where the invariant energy in first chance NN collisions is $\sqrt{s} \approx 5$ GeV, which is far above threshold and where the production cross section changes only smoothly with energy (cf. Fig. 7). Furthermore, due to higher meson densities also meson-meson reaction channels will become important especially for heavy systems such as Au + Au.

We will investigate the same systems as in Section 3.1 where we have concentrated on proton and pion rapidity distributions that we were found to be reasonably in line with the HSD transport calculations. We start with p + Be at 14.6 GeV and display in Fig. 13 (l.h.s.) the calculated K^+ and K^- rapidity distributions in comparison to the data of the E802 Collaboration [47]. Both K^+ (upper line) and K^- rapidity distributions (lower line) are almost symmetric around midrapidity indicating little reabsorption of both mesons due to the small size of the target. The K^+ and K^- spectra are described quite well by the calculation using $\gamma_s = 0.4$ (solid lines). We also show in Fig. 13 (l.h.s.) the results calculated with a strangeness suppression factor γ_s=0.3 (dotted lines) taken for the hadronization of the strings, which underestimates the data by roughly 30%. For that reason γ_s=0.4 is taken in the HSD approach as mentioned in Section 2.2 in order to explain essentially p + p (or p + Be) reactions as input.

The calculated K^+ and K^- spectra for p + Au at 14.6 A·GeV - shown in Fig. 13 (r.h.s.) - are no longer symmetric around midrapidity due to rescattering and especially K^- absorption on target nucleons. Both spectra from the E802 Collaboration [47] are not really well described by the transport approach. The K^+ yield, slightly enhanced compared to p + Be, is underestimated by $\approx 5-10\%$ whereas the K^- yield is slightly overestimated for $y_{lab} \geq 1.6$. This already might indicate that kaon production at AGS energies is not perfectly understood for p + A reactions.

How does the situation look like in light nucleus-nucleus collisions? The K^+ and K^- rapidity distributions for central Si + Al reactions at 14.6 A·GeV are shown in Fig. 14 (l.h.s.) in comparison to the data from [48]. Here the K^+ yield as well as the K^- yield are *underestimated* by roughly 20-30%! In this rather light system there is only a small amount of rescattering, since most secondary particles are produced (after their formation time) in the vacuum. This indicates that the primary production mechanism of kaons and antikaons is not sufficiently described within our hadronic model!

The situation becomes worse for Si + Au at 14.6 A·GeV as shown in Fig. 14 (middle) where our calculations underpredict the K^+ and K^- rapidity distributions

significantly from E802 and E859 [48, 57]. The situation is similar for the RQMD approach for Si + Au as demonstrated in Fig. 8 of Ref. [28]. Whereas RQMD also overestimates the π^+ and π^- spectra slightly [28], the K^+/K^- ratio and especially the K^+/π^+ ratio is underestimated sizeably in comparison to the data from E802. Since strangeness is conserved in both calculations (RQMD and HSD) we have to conclude here that the initial production of strangeness, i.e. $\bar{s}s$ pairs, is underestimated in the hadronic models.

The heaviest system studied at the AGS is Au + Au at ≈ 11 A·GeV. Our calculated kaon and antikaon rapidity spectra for semicentral (5-12%) reactions (1.5 fm $\leq b \leq$ 3.0 fm) are displayed on the r.h.s. in Fig. 14 in comparison to the data from Ref. [58]. Again we underestimate the kaon yield by roughly 30 %. We note that this is also the case for most central collisions, which are not shown here.

In view of the systematic presentation of our results in comparison to data from p + Be to Au + Au collisions we infer that the hadronic transport model does not accurately enough describe the strangeness production in these systems as to allow for definite conclusions. Furthermore, independent calculations within the ART-code from Li and Ko [14] seem to describe the K^+ spectra for central Au + Au reactions. Unfortunately, the latter calculations have not been applied to the other systems (p + Be, p + Au, ...) presented here, such that in case of conflicting results between different transport calculations no unbiased message can be extracted.

4.2 SPS energies

Since about 2 decades the strangeness enhancement in ultrarelativistic nucleus-nucleus collisions has been proposed as a possible signature for the formation of a quark-gluon-plasma (QGP) [1]. However, strangeness is produced also in all energetic collisions of nonstrange mesons with nonstrange baryons as well as nonstrange meson-meson collisions. Thus the relative abundance of these secondary and ternary reaction channels will be of delicate importance in determining the relative $\bar{s}s$ enhancement compared to *pp* collisions at the same energy. In this respect we display in Fig. 15 the number of BB and mB collisions as a function of the invariant collision energy $\sqrt{s}$ for central S + S collisions at 200 A·GeV and Pb + Pb collisions at 160 A·GeV. The baryon distributions for both systems show moderate peaks around the initial $\sqrt{s} = (4m_N^2 + 2m_N T_{lab})^{1/2}$, but extend over the whole $\sqrt{s}$ regime with an even more pronounced peak slightly above $\sqrt{s} = 2m_N$. Whereas the first peak corresponds to the first-chance nucleon-nucleon collisions, the latter one represents low energy comover scattering. Most of the intermediate BB collisions are secondary or higher order collisions of the leading constituents of the strings, which are included in the BB distributions. Due to the larger size of the system these intermediate energy BB collisions are enhanced for Pb + Pb as compared to S + S. Meson-baryon collisions and meson-meson collisions (not shown) are about factors of 2 and 4, respectively, higher in Pb + Pb as compared to S + S. In view of the strangeness production threshold in mB reactions of 1.612 GeV for kaons and 1.932 GeV for $K\bar{K}$ pairs, respectively, still a considerable part of secondary mB reactions can contribute to the net strangeness production.

Since the Lund-string-model (LSM) describes the strangeness production in *pp* col-

lisions very well – as illustrated in Section 2.2 – and also the low energy production channels are reasonably well under control (cf. Ref. [30]), it is now a quantitative question if a hadronic model will be able to describe the strangeness production in proton-nucleus and nucleus-nucleus collisions at SPS energies. In Fig 16 we compare the HSD results to early experimental measurements of p + S and p + Au reactions by the NA35 Collaboration [59]. The p + S collisions are not truly minimun bias as p + Au, but require a minimun of five charged particles to be detected by the NA35 streamer chamber. The hyperon and K^0_S distributions for p + A collisions follow the trend in the experimental data. However, the calculated K^0_S rapidity distribution for the p + Au system is broader compared to the data and shows no peak at target rapidity. These findings are similar to results obtained within the RQMD model [29], although RQMD gets slightly more kaons and hyperons for p + A collisions, which may be attributed to a different treatment of the production and interaction of resonances at intermediate energies.

Let us turn now to heavy-ion collisions. Our results for central collisions of S + S at 200 A·GeV for the rapidity distributions of K^+ and K^- are displayed in Fig 17 in comparison to the data from the NA35 [60, 61] and NA49 Collaborations [62]. Since these data as well as the corresponding pion rapidity distributions (cf. Fig. 11) are described quite reasonably in the hadronic transport approach, the quoted strangeness enhancement can also be explained in a hadronic scenario including rescattering. This has been pointed out by Sorge since a couple of years [63]; our independent calculations thus support his findings.

For the light system S + S about 90% of K^+ and 82% of K^- stem from BB collisions whereas the contribution from mB reactions is 6% for K^+ and 8% for K^-; 4% of K^+ arise from mm reactions and about 7% of K^- mesons. The residual K^- seen asymptotically stem from πY channels. Since in Pb + Pb collisions these secondary and ternary reactions are more frequent, one might expect an even stronger enhancement of strangeness production for the heavier system.

Our results for the kaon and antikaon rapidity distributions for central collisions of Pb + Pb at 160 A·GeV are shown in Fig. 17 (r.h.s.) in comparison to the data from [62]. As for S + S at 200 A·GeV the K^+, K^- distributions are reproduced rather well. The calculated Λ rapidity distribution (dotted line in Fig. 17) is fixed by the kaon yield due to strangeness conservation but it underestimates slightly the NA49 data [62] (open triangles) at midrapidity.

Contrary to S + S reactions the kaon production by mB channels for Pb + Pb collisions increases to about 20% and mm channels give roughly 15% in case of K^+ mesons. Antikaons, that are detected finally, stem from BB collisions by $\approx$ 52%, further 20% come from mB reactions, 13% from mm channels and 15% from πY channels which indicates the relative importance of secondary and ternary reactions for the heavy system. Thus the strangeness enhancement in the kaon and Λ-particle sector seen at SPS energies appears to be compatible with a hadronic reaction scenario.

5 Stepping down to SIS energies

A further test of strangeness production is to study the energy range between AGS and SIS energies (1-2 A·GeV). At SIS energies the HSD approach describes the data for kaon (K^+) production rather well [30, 31] even without including selfenergies, since the kaon potential should only be slightly repulsive. To illustrate this we show in Fig. 18 the K^+ rapidity spectra for Ni + Ni collisions at 1.93 AGeV in comparison to the data from the FOPI Collaboration [64]. As in Ref. [31] the K^+ yield is well described without including any medium effects for the kaons.

The E866 and E895 Collaborations recently have measured Au + Au collisions at 2,4,6 and 8 A·GeV kinetic energy at the AGS. Thus it is of particular interest to look for a *discontinuity in the excitation functions* for pion and kaon rapidity distributions and to compare them to our hadronic model. In Table 2 the K^+/π^+ ratios for central (b=2 fm) Au + Au collisions at 2,4,6,8 and 11 AGeV are shown together with the preliminary data. The ratio at midrapidity $\frac{|y-y_{CM}|}{y_{CM}} < 0.25$ is slightly higher, because the kaon rapidity distribution is narrower than that of the pions. While the scaled kaon yield at 2 AGeV (SIS energies) is described in the HSD approach within the experimental errorbars, the experimental K^+/π^+ ratio at 4 AGeV is underestimated already by a factor of 2 and saturates at roughly 19% for 11 AGeV.

Recent RQMD calculations [19, 58] obtain higher K^+/π^+ ratio in the energy range 2-11 A·GeV for Au + Au collisions, which are even above the experimental values. The strong increase compared to earlier RQMD versions [28] results from some conceptual new steps in the meson-baryon sector as described in [16]. As mentioned before, an analysis for different systems over the complete energy range would be helpful for a quantitative comparison of the different approaches.

The difference of the calculated scaled kaon yield and the data for the Au + Au collisions at 2-11 AGeV may be connected with an overestimate of the pion yield, an underestimate of the kaon yield or an admixture of both in the HSD approach. In this context we show in Fig.19 our predictions of the excitation function of the π^+ and K^+ rapidity distributions for central (b=2 fm) Au + Au collisions at 2,4,6,8 and 10 A·GeV. A comparison with data – to come up in the near future – will clarify the question about pion excess and/or missing strangeness.

6 Summary

We have presented a systematical study of strangeness production from SIS to SPS energies for different systems using the HSD approach in the cascade mode. An important ingredient of the present analysis are the elementary cross sections for strangeness production in baryon-baryon, meson-baryon and meson-meson channels, which have been discussed in detail and are in good agreement with the experimental data. In order to avoid (partly unknown) parameters, neither vector or scalar fields are included for the baryons nor any selfenergies of mesons. In this respect our investigations have to be seen as a rather conservative approach. Furthermore, only baryon resonances up to $N^*(1535)$ are included since most of the properties of higher resonances in dense

hadronic matter are unknown, in particular their decay into the strangeness sector ($N^* \rightarrow KY$ or $m^* \rightarrow K\bar{K}$) and their width, which are expected to be broadened substantially in the hadronic environment. In the present approach the corresponding excitations of baryons and mesons are described by strings. Their decay into the strangeness channels and especially the K/π ratio in the final state is given by a single parameter γ_s and fixed to experimental p + p and π^+ + p data.

We found an enhancement of the scaled kaon yield in heavy-ion collisions due to hadronic rescattering both with increasing system size and energy. It should be emphasized that this is expected within any hadronic model: After the primary string fragmentation the hadronic fireball starts with a K^+/π^+ ratio far below chemical equlibrium with $\approx 6\%$ ($\approx 8\%$) at AGS (SPS) energies before the hadronic rescattering starts. The average kinetic energy and the particle density increases monotonically with incoming kinetic energy of the projectile while the life time of the fireball increases with the system size. Thus a smooth and continuous enhancement is expected within a hadronic model by these effects.

To summarize our results at AGS energies, we show in Table 3 the calculated K^+ and π^+ yield (integrated over the full rapidity space) as well as the K^+/π^+ ratio from HSD for different systems in comparison to the experimental ratios from Ref. [47]. Allready for Si + Al the HSD approach overestimates the pion yield by roughly 15%, as shown in Section 3.1, and underestimates the kaon and antikaon yield by $\approx 30\%$. Thus the calculated scaled kaon yield K^+/π^+ is essentially too low as shown in the last two columns of Table 3. While the experimental ratio increases by a factor of 3 from p + p to central Au + Au collisions, the HSD appoach gives only a factor of 1.5. Our conclusions are similar to the findings in the RQMD model [28] for the system Si + Au, where a ratio E802/RQMD of 0.83 (in the rapidity interval $0.6 < y < 2.8$) for π^+ and 1.22 for K^+ ($0.6 < y < 2.2$) was found. This corresponds to a ratio $(K^+/\pi^+)_{RQMD} \approx 11.5\%$, which is slightly higher than the HSD result. This may be connected with different rapidity cuts, because the pion rapidity distribution is broader than that of the kaons. Our value of 9 % is obtained by integrating over full rapidity space while the values of RQMD are taken around midrapidity. The difference between the resonance picture of RQMD and the string picture of HSD seems to be rather small; however, there is a sizeable discrepancy between the cascade results (of RQMD and HSD) and the data.

Furthermore, the shape of the experimental pion rapidity distributions is narrower for A + A collisions compared to p + p collisions, which is also not described by the hadronic transport model. This result again is in agreement with findings in the RQMD model (c.f. Fig. 6 of Ref. [28]) and with the ARC model [13]. Both observables, the strong enhancement of the scaled kaon yield as well as the lowering of the width of the pion rapidity distribution, are already found for the rather light system Si + Al (see Fig. 9 and Fig. 14), where the amount of hadronic rescattering is rather small. Thus the shape of the pion rapidity distribution in Si + Al reactions and the strangeness yield is dominated by the primary string fragmentation process, which on the other hand is fixed by p + p and p + Be data. The difference of p + Be and Si + Al collisions is hard to understand within a hadronic rescattering scenario and might indicate new physics for the primary $s\bar{s}$ production mechanism at AGS energies.

On the other hand, the production of pions, kaons and antikaons as well as the stopping of the incident protons at SPS energies is in line with the hadronic transport approach. To illustrate this we summarize in Table 4 the calculated kaon, antikaon and pion yield and the scaled kaon yield

$$\frac{<K>}{<\pi>} = \frac{<K^+ + K^- + K^0 + \bar{K^0}>}{<\pi^+ + \pi^- + \pi^0>} \tag{20}$$

in comparison with the experimental ratios from Ref. [62]. The last two columns show a good agreement between the HSD results and the data. Thus the signal of 'strangeness enhancement' in A + A collisions at SPS energies does not qualify as a sensitive observable for an intermediate QGP phase. Nevertheless, the experimentally observed strong increase of the antihyperon and multistrange baryon yield [65] in heavy-ion collision cannot be described by our hadronic model, since no string fusion (as in the RQMD version of Ref. [16]) is included to enhance this yield. Furthermore, only the annihilation of antihyperons is include so far and not the inverse production channels like e.g. $\rho + K + \bar{K} \rightarrow \Lambda + \bar{\Lambda}$ due to technical reasons. The aim of our work was to present a systematic analysis of strangeness production (mainly kaons) over a wide range in energy and system mass $A_1 + A_2$.

In order to discuss the strangeness production over the complete energy range we also show in Table 4 the calculated K^+/π^+ ratio, which experimentally is substantially lower at SPS energies ($\approx$ 13.5%) compared to AGS energies ($\approx$ 19%) for the most heavy systems. At SPS energies this ratio is only enhanced by a factor 1.75 for central Pb + Pb collisions compared to p + p reactions and should be compared to the factor ≈ 3 at AGS. Such a decrease of the scaled kaon yield from AGS to SPS energies is hard to obtain in a hadronic transport model. On the contrary, the higher temperatures and particle densities at SPS energies allways tend to enhance the K^+/π^+ yield closer to its thermal equlibrium value of $\approx 20-25\%$ [23, 26] at chemical freezeout and temperatures around $T \approx 150$ MeV.

Our findings have to be compared to results obtained by other microscopic approaches. At AGS energies there exist calculations from RQMD within different versions [19, 28] and from ARC [13] for the system Si + Au. The earlier RQMD and ARC models agree with the presented results concerning the overestimation of the pion yield. In the kaon production there is a clear difference: While RQMD [28] also underpredicts the kaon yield by roughly 22% (HSD by 30%) the ARC code describes the kaon data rather well. Unfortunately the ARC code is fine tuned to heavy-ion collisions at AGS energies. It would be interesting to investigate whether a reduction of the scaled kaon yield at higher energies is also described within this approach. At SPS energies the investigations of strangeness production within standard RQMD and VENUS give similar results as the HSD approach. In order to account for the observed and large strange antibaryons abundancies and multi-strange baryon abundancies [65] conceptual new steps like string fusion were introduced as mentioned above. Unfortunately, no systematic analysis over the complete energy range exists from the other models. It would be of particular interest to compare a systematic study of the scaled kaon yield calculated by independent approaches to achieve a model independent conclusion on the topic of strangeness production.

Au + Au collisions at AGS for different energies			
$< K^+ > / < \pi^+ >$ [%]			
E_{lab} [AGeV]	HSD, full rapidity	HSD, $\frac{\lvert y - y_{CM} \rvert}{y_{CM}} < 0.25$	preliminary data [58]
2	3.3	3.6	4 ± 1
4	5.6	5.9	11 ± 1
6	7.6	8.0	14.5 ± 1.5
8	8.7	9.1	17 ± 1
11	9.0	9.7	19 ± 1

Table 2: The K^+/π^+ yield for Au + Au at different incident energies obtained within the HSD approach in comparison to the experimental data from Ref. [58].

Our systematic study of kaon production from SIS to SPS energies within a hadronic model shows a continuous increase of the K^+/π^+ ratio ($\approx 3.3\%$ at SIS, $\approx 9.5\%$ at AGS, $\approx 14\%$ at SPS) with energy because the average kinetic energies and particle densities rise with incident energy and enhance the scaled strangeness yield. On the other hand the energy dependence of the experimentally observed K^+/π^+ ratio in the most heavy systems rises from $\approx 3.3\%$ at SIS energies to $\approx 19\%$ at AGS and drops to $\approx 14\%$ at SPS. The high value observed at AGS might indicate the presence of a nonhadronic phase, which seems to be close to chemical equlibrium for strangeness. On the other side, strange antibaryon enhancement at SPS energies might indicate nonhadronic effects also at SPS energies, but the small K/π ratio (in comparison to AGS) shows that the system is not really in full chemical equlibrium for strangeness. In this context the study of strange antibaryons at AGS energies is of particular interest. The E859 Collaboration has measured the $\bar{\Lambda}/\bar{p}$ ratio in Si + Al at 14.6 A·GeV and has recently reported a large value $\bar{\Lambda}/\bar{p} = 2.9 \pm 0.9 \pm 0.5$ for $1.15 < y < 1.55$ [66], which would indeed favor a scenario of (nearly) chemically saturated strange antibaryon populations at freezeout. This ratio, however, cannot be reached by far within hadronic cascade-type models.

Strangeness at AGS				
system	$<K^+>$	$<\pi^+>$	$\frac{<K^+>}{<\pi^+>}$ HSD	$\frac{<K^+>}{<\pi^+>}$ data
p + Be	0.075	1.27	0.059	0.059 ± 0.01
Si + Al	1.7	24	0.071	0.12 ± 0.01 [48]
Si + Au	5.2	63	0.084	0.17 ± 0.02 [48]
Au + Au	17.5	194	0.095	0.18 ± 0.01 [58]

Table 3: The K^+/π^+ yield for different systems at AGS energies obtained within the HSD approach in comparison to the experimental data. The experimental ratio for p + Be is estimated by the E802 data [47].

Strangeness at SPS						
system	$<K>$	$<\bar{K}>$	$<\pi>$	$\frac{<K^+>}{<\pi^+>}$HSD	$\frac{<K>}{<\pi>}$HSD	$\frac{<K>}{<\pi>}$ data
p + p	0.42	0.27	9.1	0.08	0.08	0.08 ± 0.02
S + S	19.65	12.7	265	0.11	0.139	0.15 ± 0.015
S + Au	53	33.2	678	0.118	0.13	0.13 ± 0.015 (for S + Ag)
Pb + Pb	194	115	2065	0.138	0.15	0.14 ± 0.02

Table 4: The kaon $<K>=<K^+ + K^0>$, antikaon $<\bar{K}>=<K^- + \bar{K^0}>$ and pion $<\pi>=<\pi^+ + \pi^- + \pi^0>$ yield at SPS energies and the $<K^+> / <\pi^+>$ and $<K> / <\pi>=<K^+ + K^- + K^0 + \bar{K^0}> / <\pi^+ + \pi^- + \pi^0>$ ratio obtained by the HSD approach compared to the corresponding experimental ratio taken from Ref. [62].

References

[1] J. Rafelski and B. Müller, Phys. Rev. Lett. 48 (1982) 1066; Phys. Rev. Lett. 56 (1986) 2334; T. S. Biro and J. Zimanyi, Nucl. Phys. A 395 (1983)525;

[2] P. Koch, B. Müller and J. Rafelski, Phys. Rep. 142 (1986) 167. P. Koch, Z. Phys. C 38 (1988) 269.

[3] J. Rafelski, J. Letessier and A. Tounsi, Acta. Phys. Polonica B 27 (1996) 1035.

[4] T. S. Biro, P. Levai and B. Müller, Phys. Rev. D 42 (1990) 3078.

[5] See e.g., 'Strangeness in Quark Matter '97, J. Phys. G 23 (1997).

[6] W. Ehehalt and W. Cassing, Nucl. Phys. A 602 (1996) 449.

[7] B. Anderson, G. Gustafson and Hong Pi, Z. Phys. C 57 (1993) 485.

[8] Sa Ben-Hao and Tai An, Comp. Phys. Commu. 90 (1995) 121; Phys. Rev. C 55 (1997) 2010; Phys. Lett. B 399 (1997) 29; nucl-th/9804002;nucl-th/9804003;nucl-th/9804004.

[9] K. Werner, Z. Phys. C 42 (1989) 85.

[10] H. Sorge, H. Stöcker and W. Greiner, Nucl. Phys. A 498 (1989) 567c; Ann. Phys. 192 (1989) 266.

[11] A. Capella, U. Sukhatme, C. I. Tan and J. Tran Tranh Van, Phys. Rep. 236 (1994) 225.

[12] L. V. Bravina, N. S. Amelin, L. P. Csernai, P. Levai and D. Strottman, Nucl. Phys. A 544 (1994) 461c.

[13] S. H. Kahana, D. E. Kahana, Y. Pang and T. J. Schlagel, Annu. Rev. Part. Sci. 46 (1996) 31.

[14] B. A. Li and C. M. Ko, Phys. Rev. C 52 (1995) 2037.

[15] S. A. Bass et al., nucl-th/9803035, to appear in Prog. Part. Nucl. Phys. (1998).

[16] H. Sorge, Phys. Rev. C 52 (1995) 3291; Phys. Lett. B 344 (1995) 35.

[17] K. Werner, Phys. Lett. B 308 (1993) 372.

[18] J. Aichelin and K. Werner, Phys. Lett. B 300 (1993) 158; K. Werner Phys. Rev. Lett. 73 (1994) 1594; Phys. Rev. Lett. 76 (1996) 1027.

[19] H. Sorge, Nucl. Phys. A 630 (1998) 522c.

[20] X. N. Wang, and M. Gyulassy, Phys. Rev. D 44 (1991) 3501; Phys. Rev. D 45 (1992) 844.

[21] A. Shor and R. Longacre, Phys. Lett. B 218 (1989) 100.

[22] K. Geiger, Phys. Rep. 258 (1995) 237.

[23] P. Braun-Munzinger, J. Stachel, J. P. Wessels and N. Xu, Phys. Lett. B 344 (1995) 43; Phys. Lett. B 365 (1996) 1.

[24] J. Letessier, J. Rafelski and A. Tounsi, Phys. Lett. B 292 (1992) 417; J. Letessier et al., Phys. Rev. D 51 (1995) 3408.

[25] J. Sollfrank and U. Heinz, *Quark Gluon Plasma 2*, ed. R. C. Hwa (Singapore; World Scientific).

[26] C. Spieles. H. Stöcker and C. Greiner, Eur. Phys. J C2 (1998) 351.

[27] D. E. Kahana and S. H. Kahana, nucl-th/9804017.

[28] M. Gonin et al., Phys. Rev. C 51 (1995) 310; R. Matiello, H. Sorge, H. Stöcker and W. Greiner, Phys. Rev. Lett 63 (1989) 1459.

[29] H. Sorge et al., Z. Phys. C 59 (1993) 85.

[30] W. Cassing, E. L. Bratkovskaya, U. Mosel, S. Teis and A. Sibirtsev, Nucl. Phys. A 614 (1997) 415.

[31] E. L. Bratkovskaya, W. Cassing and U. Mosel, Nucl. Phys. A 622 (1997) 593.

[32] W. Cassing, W. Ehehalt, and C. M. Ko, Phys. Lett. B 363 (1995) 35; W. Cassing, W. Ehehalt, and I. Kralik, Phys. Lett. B 377 (1996) 5; E. L. Bratkovskaya, W. Cassing and U. Mosel; Z. Phys. C 75 (1997) 119; E. L. Bratkovskaya and W. Cassing, Nucl. Phys. A 619 (1997) 413; W. Cassing and E. L. Bratkovskaya, Nucl. Phys. A 623 (1997) 570.

[33] Gy. Wolf, W. Cassing, W. Ehehalt and U. Mosel, Prog. Part. Nucl. Phys. 30 (1993) 273.

[34] The Particle Data Group, Phys. Rev. D 50 (1994) 1175.

[35] J. Geiss et al., nucl-th/9803008.

[36] B. Anderson, G. Gustafson, G. Ingelmann and T. Sjörtrand, Phys. Rep. 97 (1983) 31.

[37] J. Schwinger, Phys. Rev. 82 (1951) 664.

[38] V. Blobel et al., Nucl. Phys. B 69 (1974) 454.

[39] C. DeMarzo et.al., Phys. Rev. D 26 (1982) 1019.

[40] B. Alper et al. Nucl. Phys. B 100 (1975) 237.

[41] A. Baldini, V. Flaminio, W. G. Moorhead and D. R. O. Morrison, Landolt-Börnstein, New Series, Vol.12 (1988) (Springer-Verlag, Berlin).

[42] T. Kafka et al., Phys. Rev. D 16 (1977) 1261.

[43] G. Giacomelli, Int. J. Mod. Phys. A 5 (1990) 223.

[44] J. T. Balewski et al., nucl-ex/9803003.

[45] W. Oelert et al., nucl-ex/9803004.

[46] K. Tsushima, S. W. Huang and A. Fässler, J. Phys. G 21 (1995) 33; Phys. Lett. B 337 (1994) 245.

[47] T. Abbott et al., E802 Collaboration, Phys. Rev. C 47 (1993) 1351.

[48] T. Abbott et al., E802 Collaboration., Phys. Rev. C 50 (1994) 1024.

[49] Y. Akiba et al., E866 Collaboration, Nucl. Phys. A 610 (1996) 139c.

[50] L. Ahle et al., E877 Collaboration, Phys. Rev. C 57 (1998) 466.

[51] J. Baechles et al., NA35 Collaboration, Phys. Rev. Lett. 72 (1994) 1419.

[52] S. E. Vance, M. Gyulassy and X. N. Wang, nucl-th/9802036.

[53] K. Werner, Phys. Rep. 232 (1993) 87.

[54] R. Bauer et al., Nucl. Phys A 566 (1994) 87c.

[55] R. Santo et al., Nucl. Phys A 566 (1994) 61c.

[56] S.V. Afanasiev et al., NA49 Collaboration, Nucl. Phys. A 610 (1996) 188c.

[57] B. A. Cole et al., Nucl. Phys. A 590 (1995) 179c.

[58] C. A. Ogilvie for the E866 and E819 Collaborations, nucl-ex/9802004.

[59] J. Bartke et al., NA35 Collaboration, Z. Phys. C 48 (1990) 191; R. Stock et al., NA35 Collaboration, Nucl. Phys. A 525 221c; A. Bamberger et al., NA35 Collaboration, Z. Phys. C 43 (1989) 25.

[60] J. Bächler et al., NA35 Collaboration, Z. Phys. C 58 (1993) 367.

[61] V. Topor Pop et al., Phys. Rev. C 52 (1995) 1618; M. Gaździcki et al., Nucl. Phys. A 590 (1995) 197c.

[62] C. Bormann et al., NA49 Collaboration, J. Phys. G 23 (1997) 1817.

[63] H. Sorge, Z. Phys. C 67 (1995) 479.

[64] N. Herrmann, Nucl. Phys. A 610 (1996) 49c; B. Hong et al., FOPI Collaboration, Phys. Rev C 57 (1998) 244.

[65] S. Abatzis et al., WA94 Collaboration, J. Phys. G 23 (1997) 1857.

[66] G. S. F. Stephans and Y. Wu, E589 Collaboration, J. Phys. G 23 (1997) 1895.

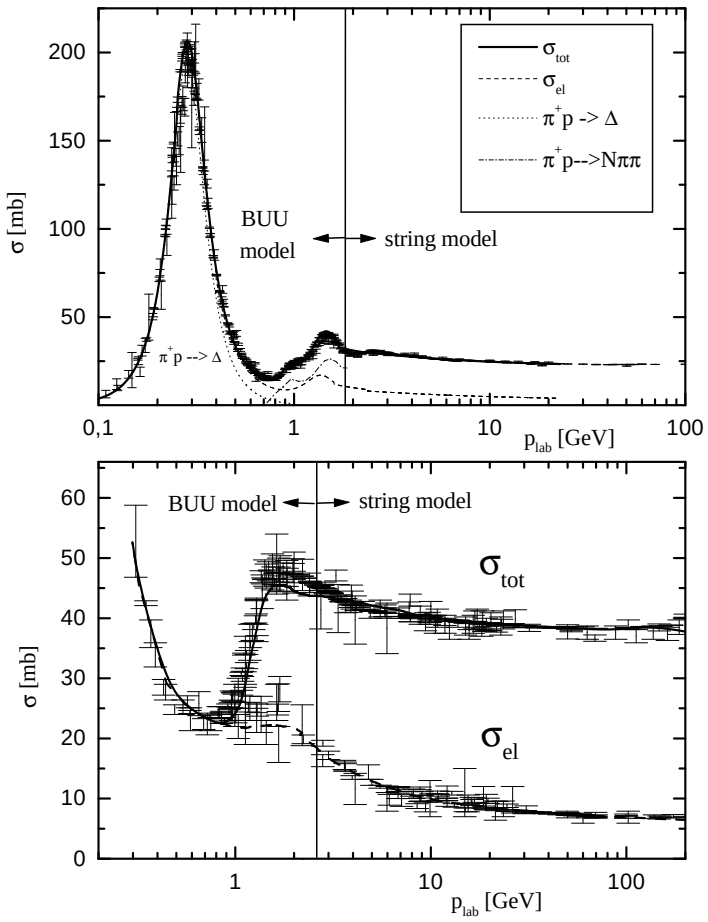

Figure 1: The total and elastic π^+-proton (upper part) and proton-proton (lower part) cross sections in comparison with the experimental data from Ref. [34]. The cross sections below the marked thresholds are taken from the BUU model [33], whereas the high energy cross sections are parametrisations of the experimental data.

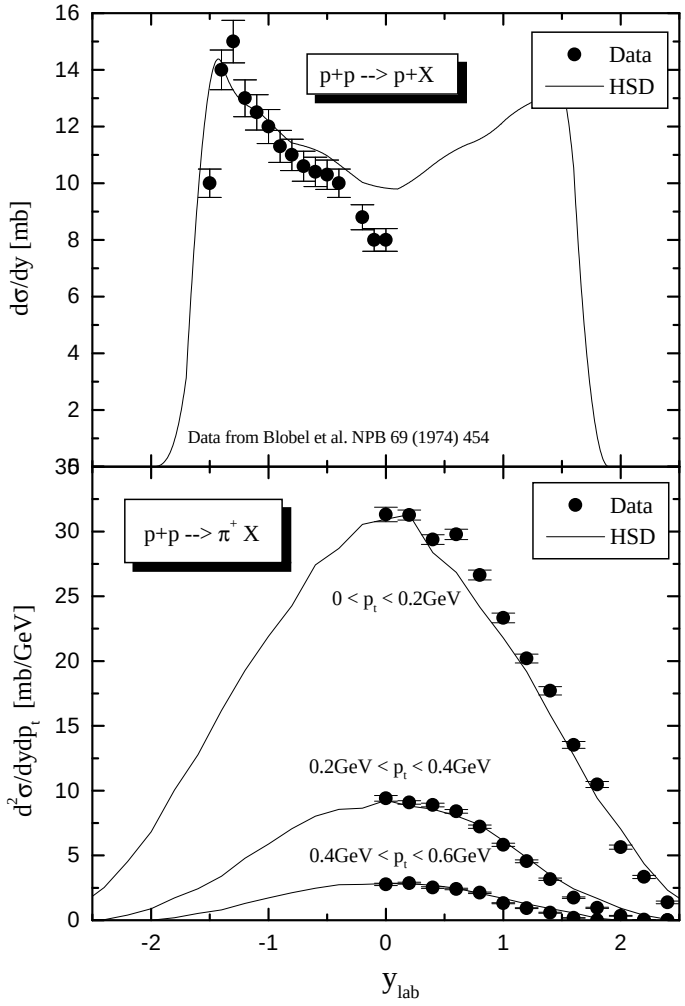

Figure 2: Invariant cross sections for inclusive proton (upper part) and π^+ production (lower part) in proton-proton collisions at $p_{lab} = 12$ GeV in comparison to the data from Ref. [38]. The π^+ results are shown for three different intervals of transverse momentum.

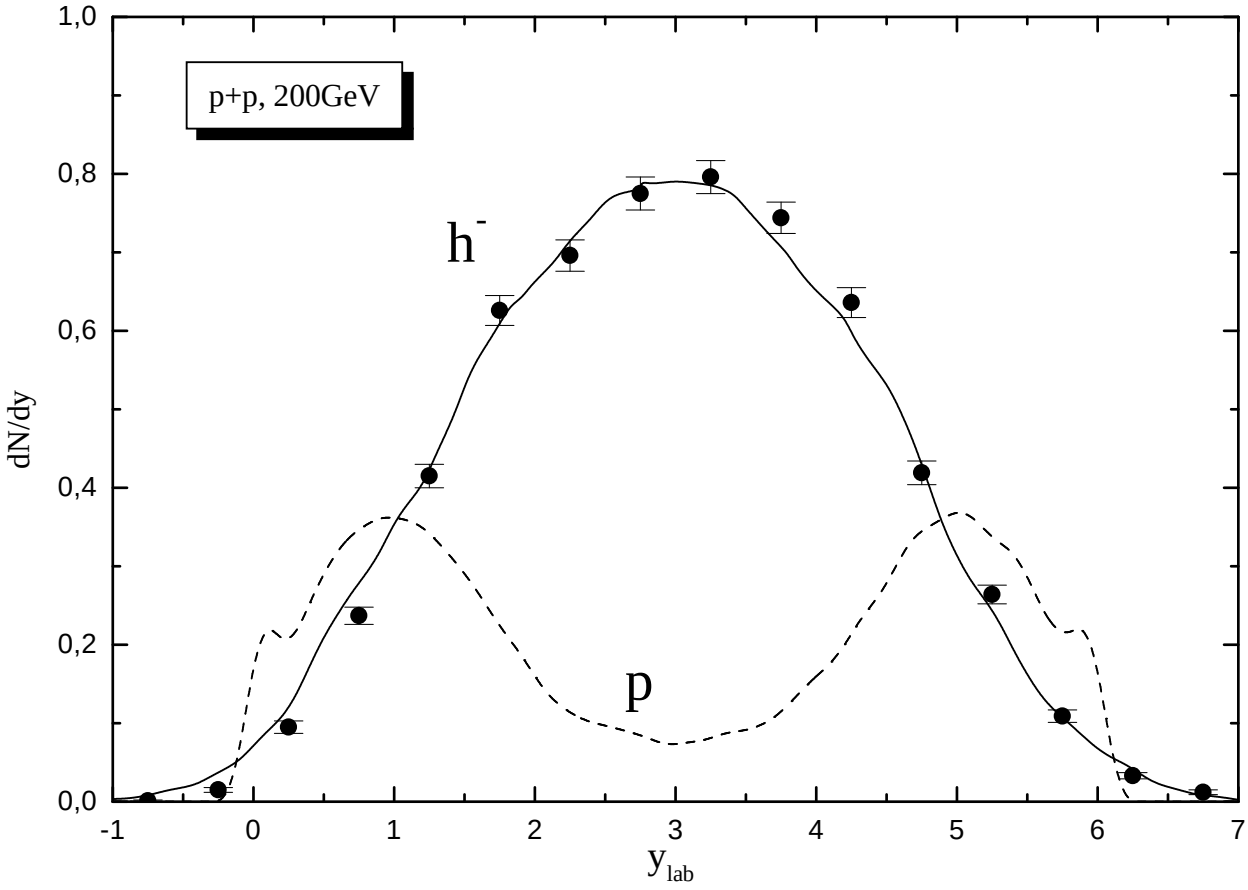

Figure 3: Rapidity distributions of protons (dashed line) and negatively charged hadrons (solid line) in proton-proton collisions at $p_{lab} = 200$ GeV in comparison to the data from Ref. [39].

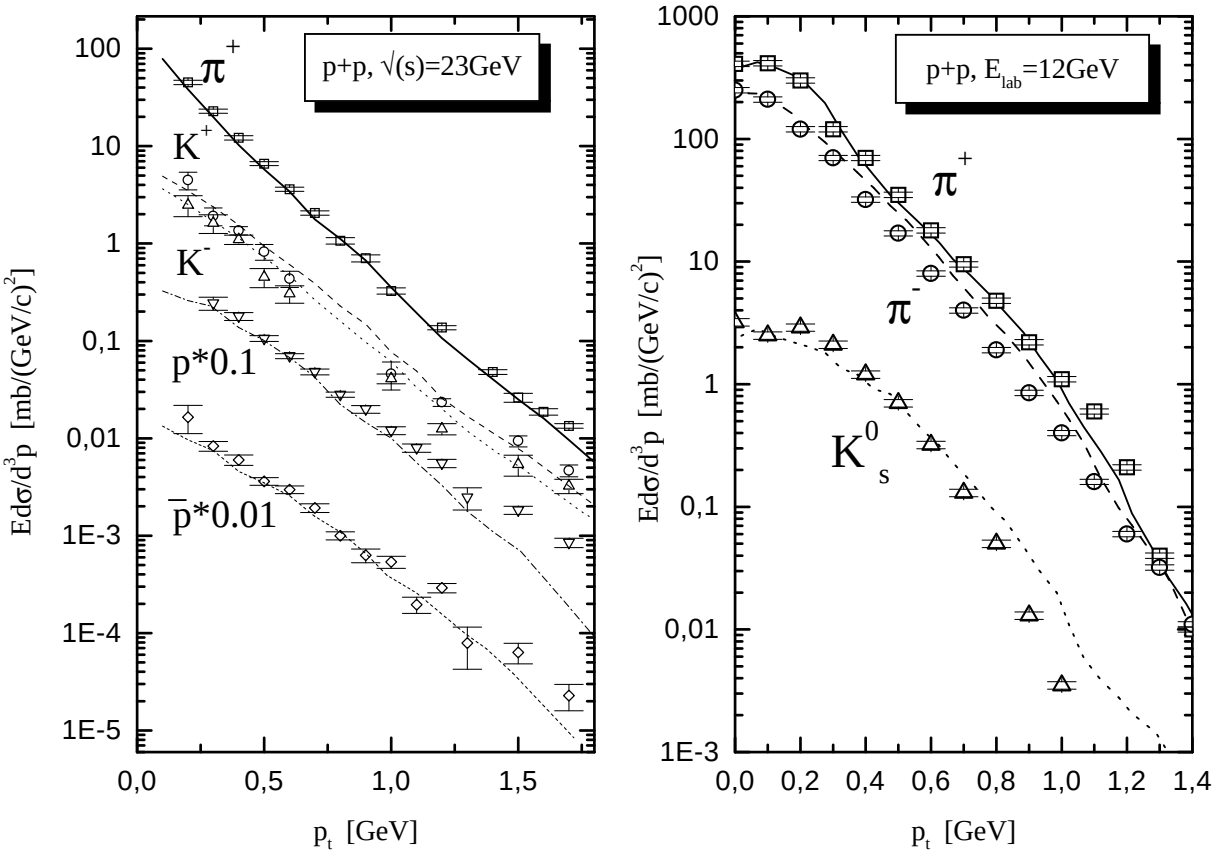

Figure 4: *l.h.s*: Transverse momentum spectra of π^+, K^+, K^-, p and $\bar{p}$ for inelastic proton-proton collisions at $\sqrt{s} = 23$ GeV (SPS energies) at midrapidity $|y| \leq 0.1$ in comparison to the data from Ref. [40]. The p and $\bar{p}$ spectra are scaled down by factors of 0.1 and 0.01, respectively. *r.h.s*: Transverse momentum spectra of π^+, π^- and K^0_s for inelastic proton-proton collisions at $p_{lab} = 12$ GeV (AGS energies). The data are from Ref. [38].

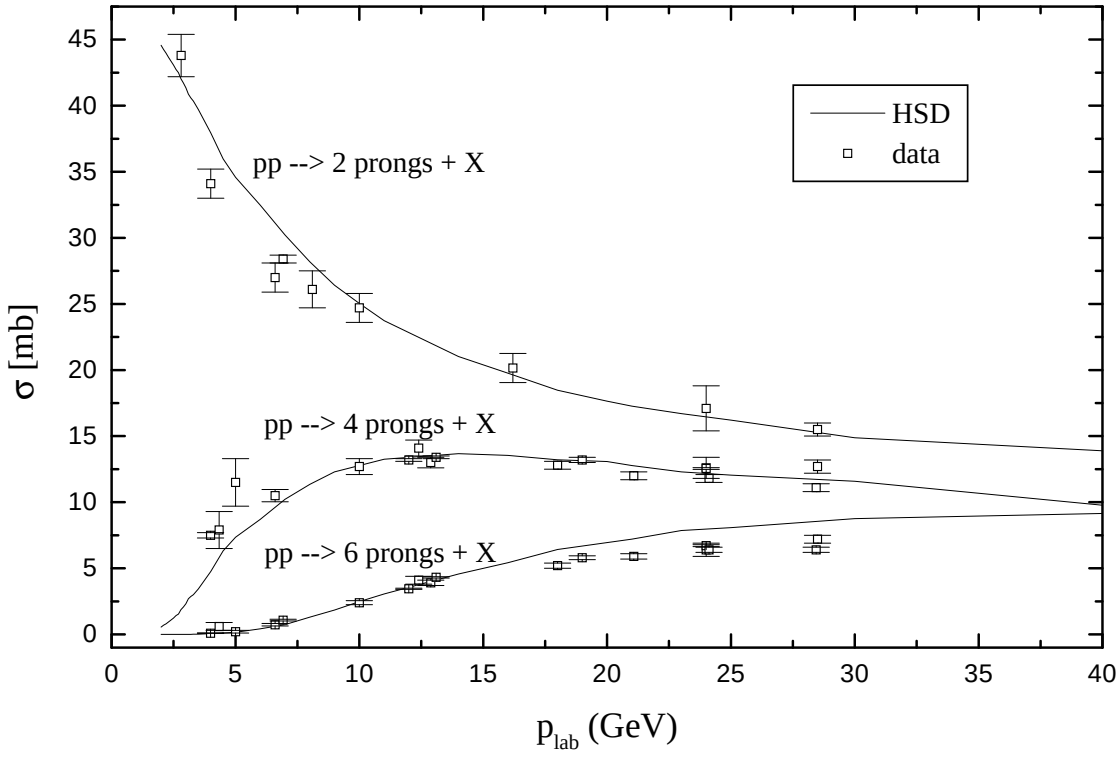

Figure 5: The energy dependent cross section for the reactions $pp \to 2prongs + X$, $pp \to 4prongs + X$ and $pp \to 6prongs + X$ in comparison to the experimental data from [41].

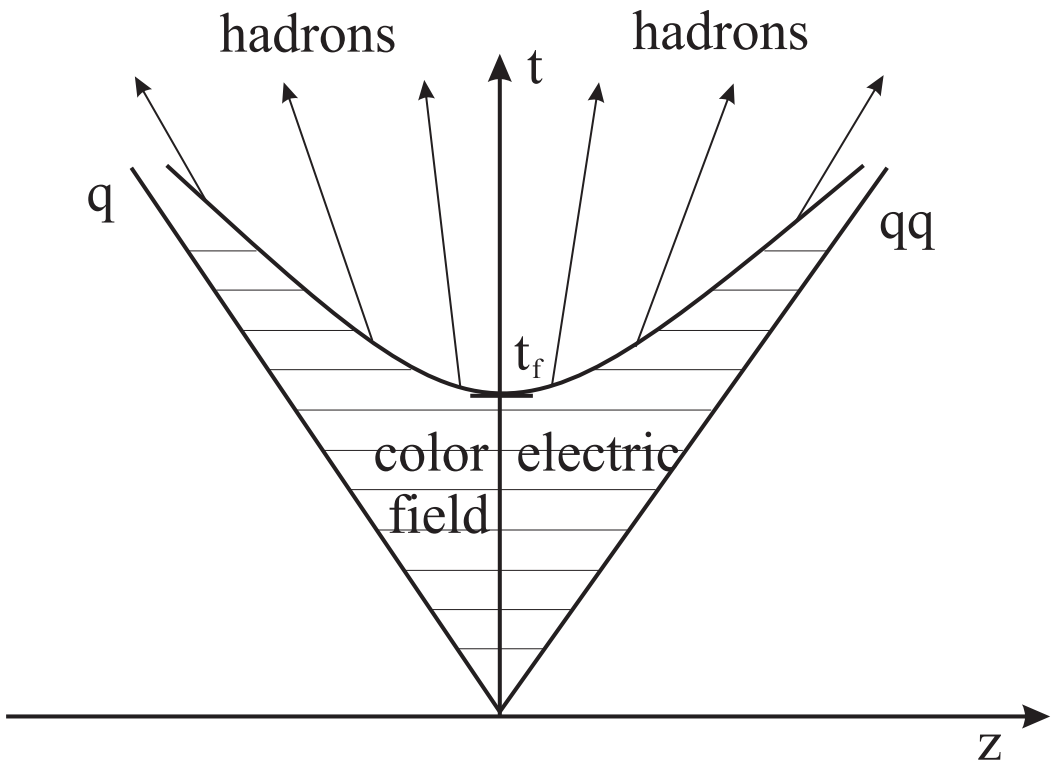

Figure 6: Dynamical evolution of a baryonic string; the fragmentation into hadrons starts after the formation time t_f.

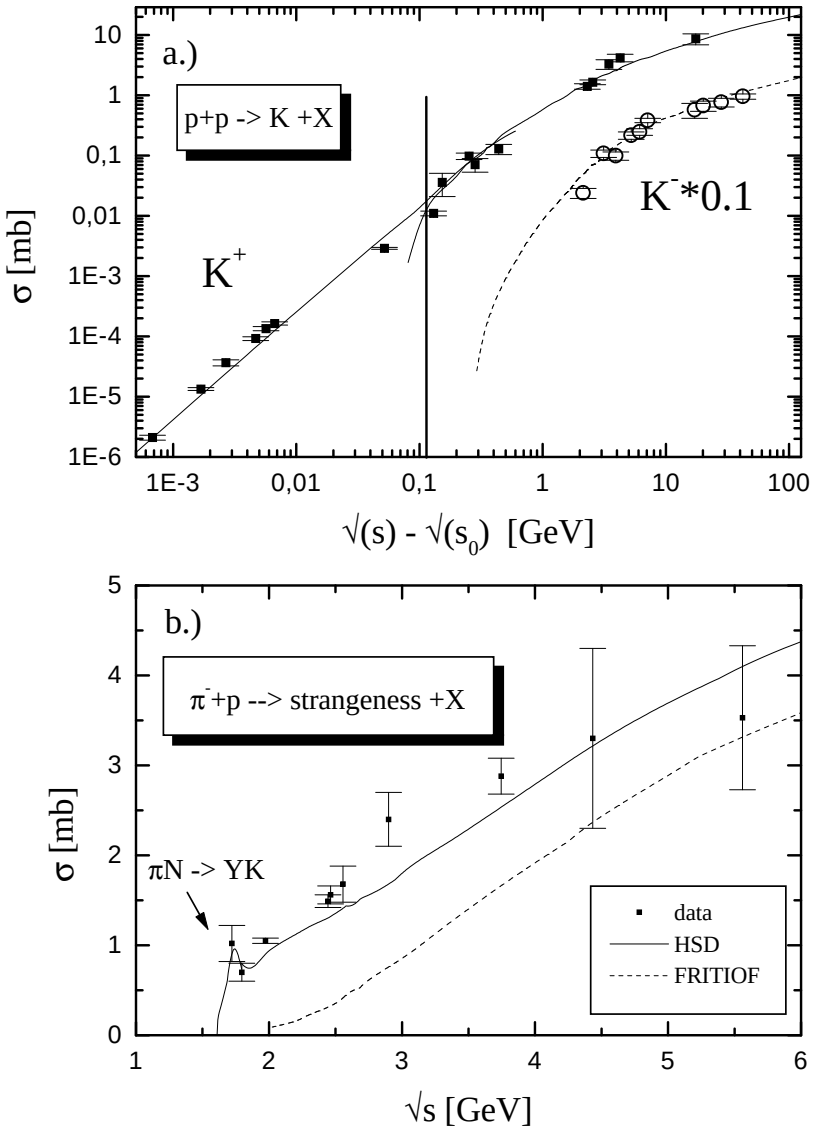

Figure 7: a.) Inclusive cross section for K^+ (full line) and K^- (dashed line, $\times 0.1$) production in p + p reactions as a function of the invariant energy above threshold in comparison to the data [43, 44, 45, 41]. For K^+ production the string threshold is marked by the solid line; below the threshold ($\approx$0.11 GeV) the parametrisations from Ref. [30] are included in the HSD code. b.) Inclusive strangeness production in π^- + p collisions in comparison with the data from [41].

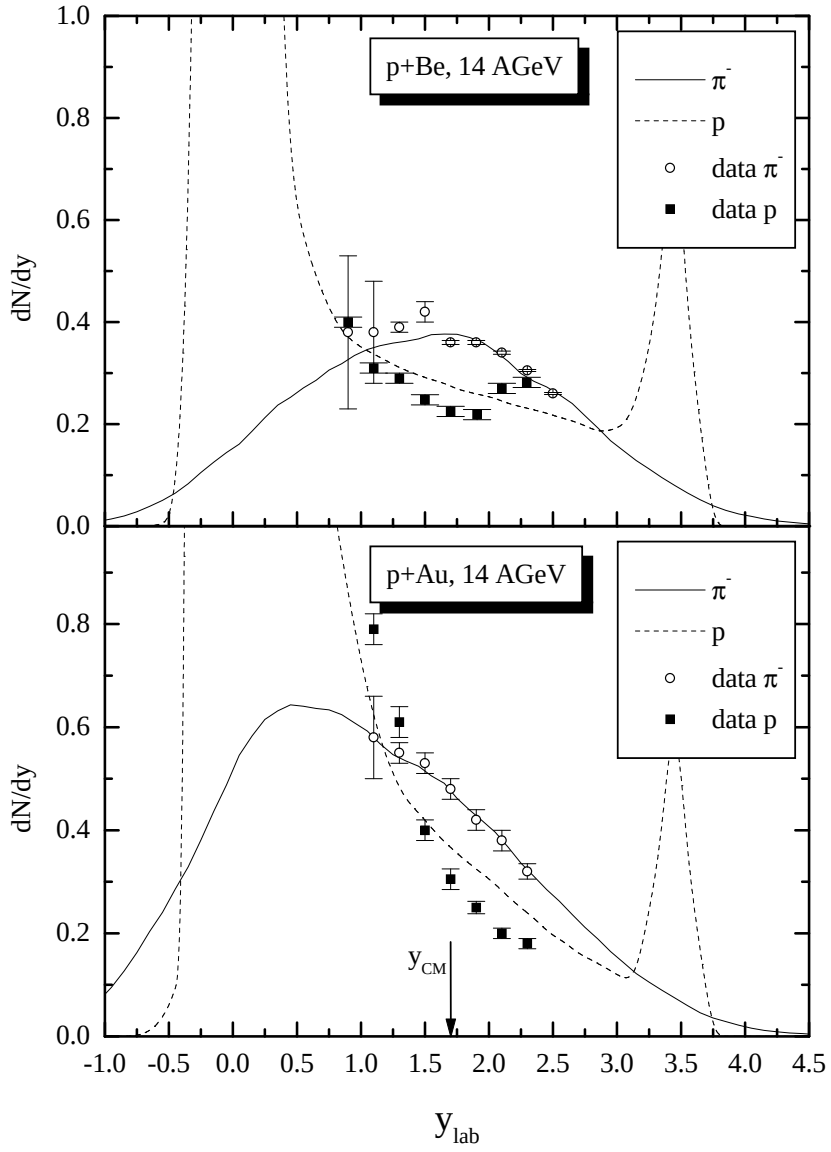

Figure 8: Inclusive proton and π^- rapidity spectra for p + Be (upper part) and p + Au (lower part) at 14.6 A·GeV in comparison to the data from the E802 Collaboration [47].

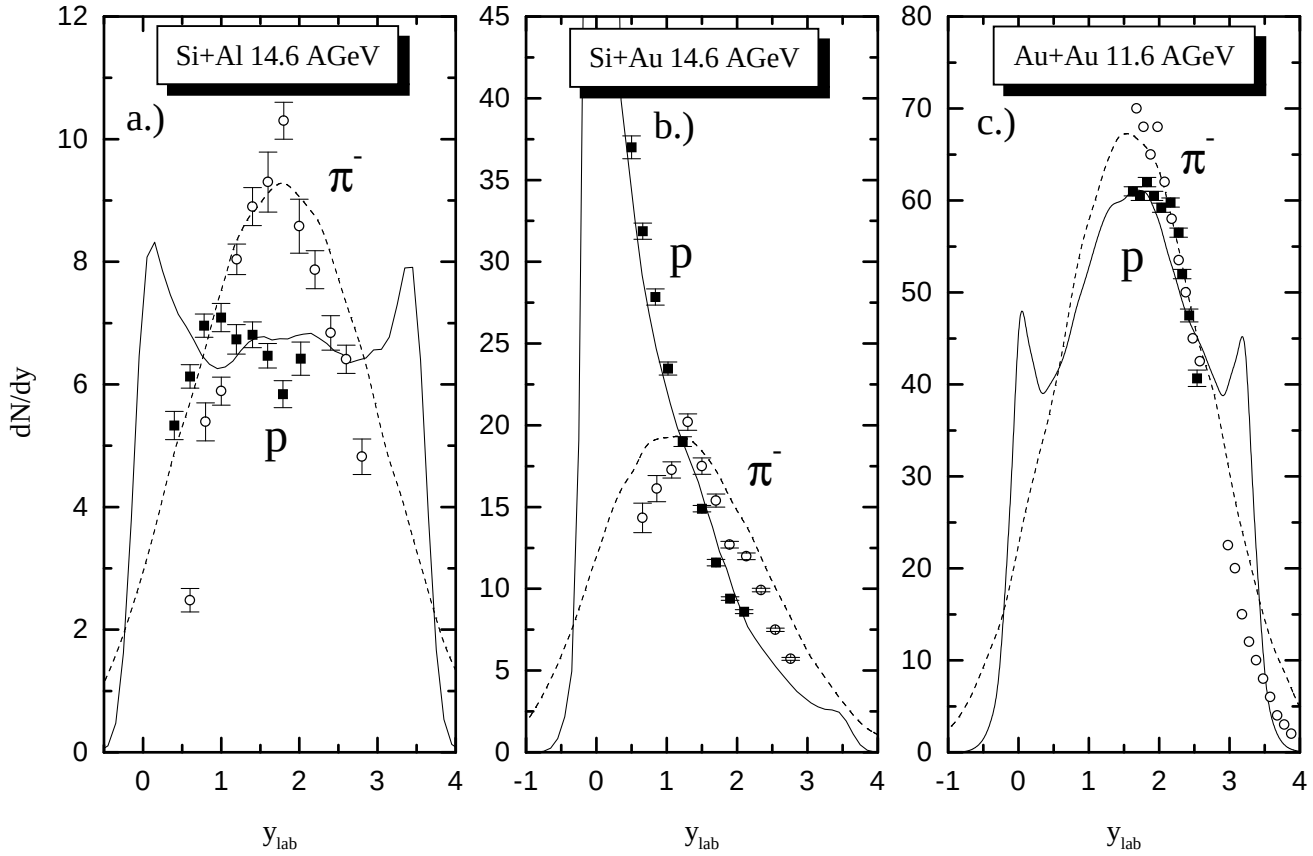

Figure 9: Inclusive proton (solid lines) and π^- (dashed lines) rapidity spectra for central Si + Al ($b \leq 1.5$ fm) at 14.6 A·GeV (left), central Si + Au ($b \leq 3$ fm) at 14.6 A·GeV (middle) and central Au + Au ($b \leq 3$ fm) at 11.6 A·GeV (right) in comparison to the data from the E802 Collaboration [48] (for Si + Al and Si + Au) and from the E866 and E877 Collaborations [49, 50].

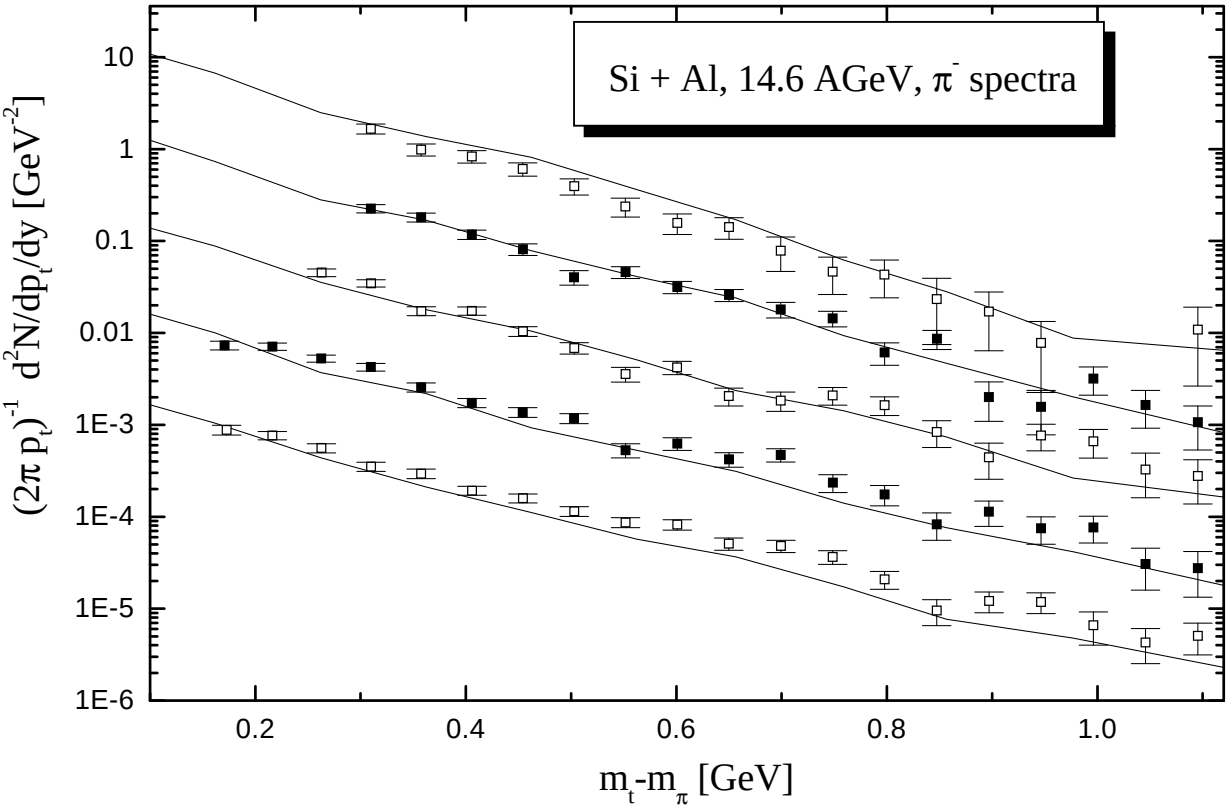

Figure 10: The transverse mass spectra $\frac{1}{2\pi p_t}\frac{d^2N}{dp_t dy}$ of π^- versus $m_t - m_\pi$ for Si + Al collisions at 14.6 AGeV. Results are shown for rapidities $y_{lab} = 0.5$, 0.7, 0.9, 1.1, 1.3 and 1.5 (from top to bottom) successively scaled down by a factor of 10. The experimental data are from Ref. [48].

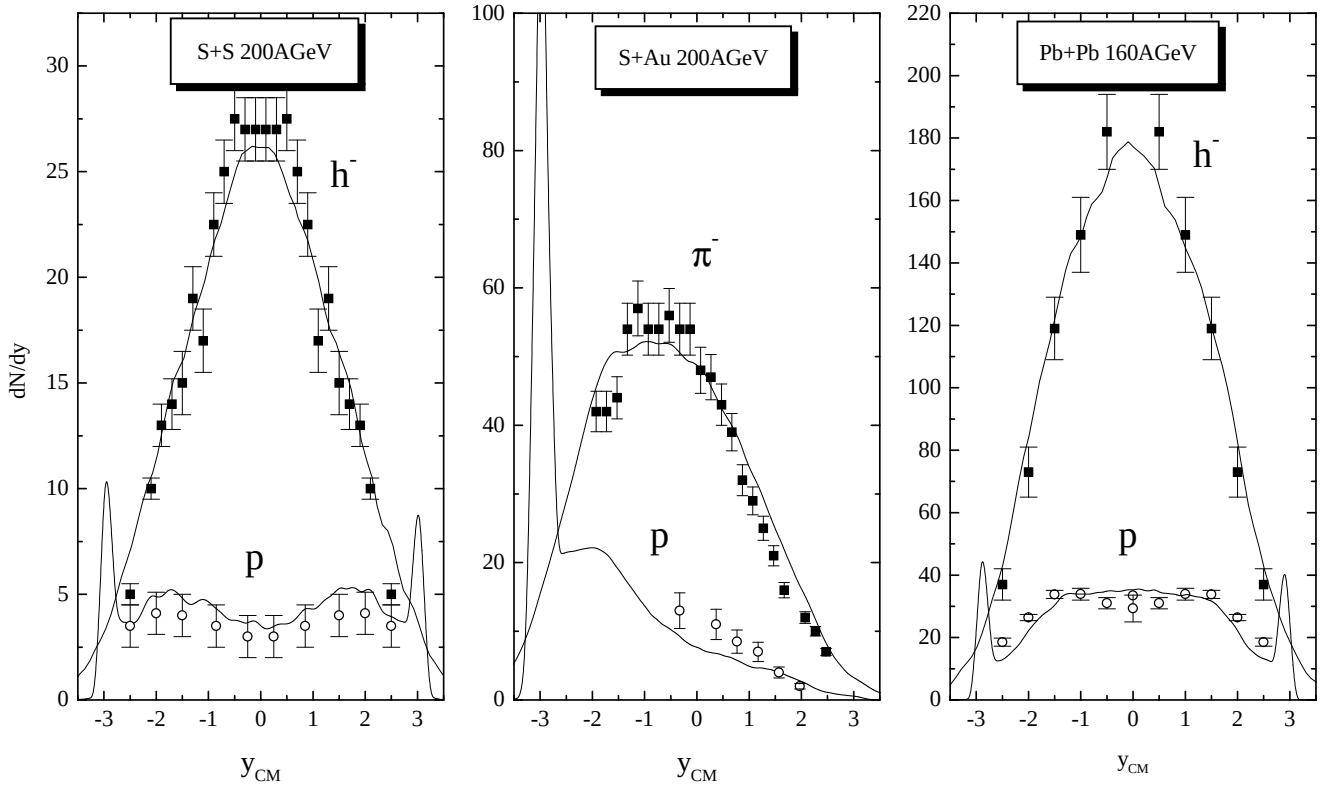

Figure 11: Inclusive proton and h^- (or π^-) rapidity spectra for central S + S collisions ($b \leq 1.5$ fm) at 200 A·GeV (left), central S + Au collision ($b \leq 2$ fm) at 200 A·GeV (middle) and central Pb + Pb collisions ($b \leq 2.5$ fm) at 160 A·GeV (right) in comparison to the data from the NA35 Collaboration [51] and the NA49 Collaboration [56].

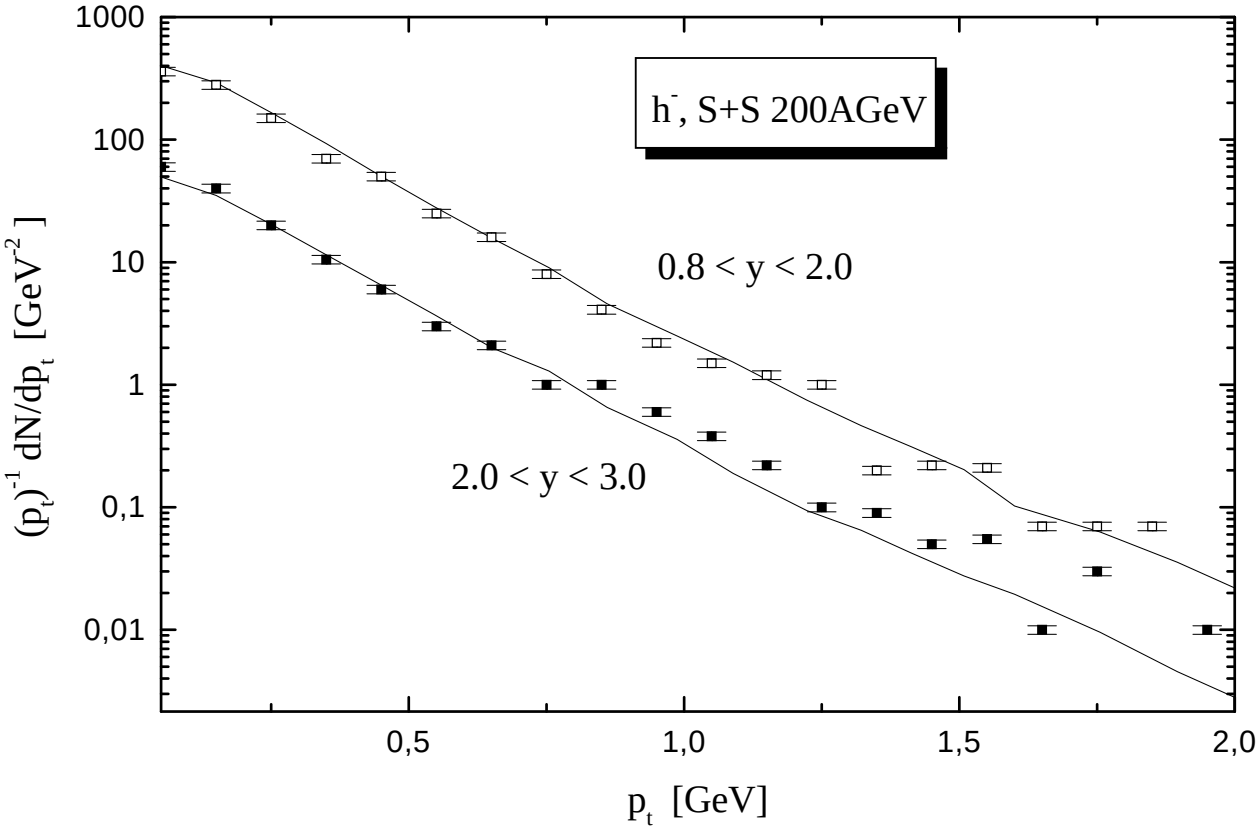

Figure 12: The transverse mass spectra $\frac{1}{(p_t)}\frac{dN}{dp_t}$ of h^- versus $m_t - m_\pi$ for S + S collisions at 200 AGeV in comparison to the experimental data from [51]. Results are shown for two cm rapidities $0.8 \leq y \leq 2.0$ and $2.0 \leq y \leq 3.0$ (lower line, multiplied by $\times 0.1$).

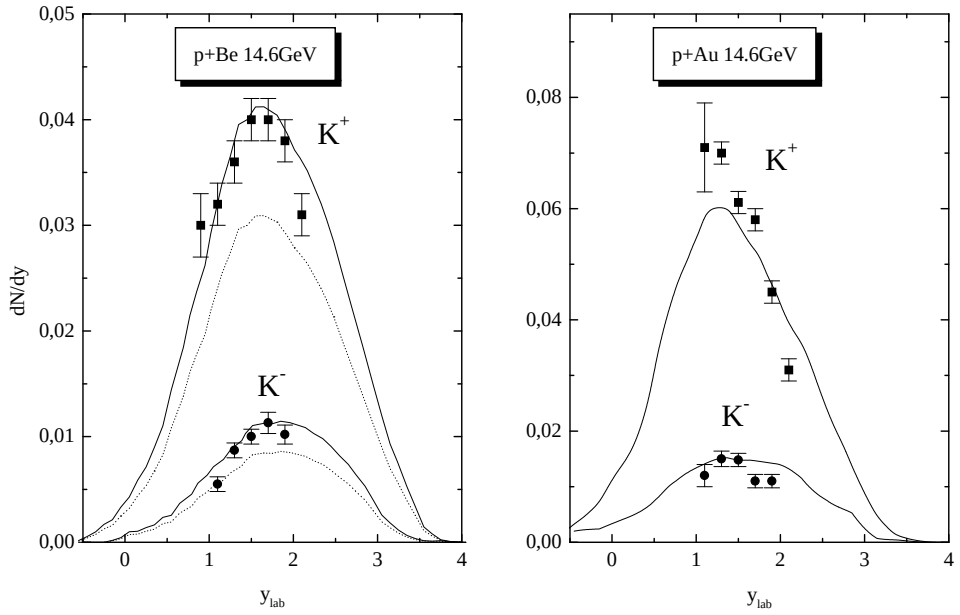

Figure 13: Calculated K^+ and K^- rapidity spectra for p + Be (l.h.s) and p + Au (r.h.s.) at 14.6 A·GeV (solid lines) in comparison to the data from the E802 Collaboration [47]. The dashed lines for p + Be are calculated with a strangeness suppression factor $\gamma_s = 0.3$ while the solid lines are obtained for $\gamma_s = 0.4$ (see text).

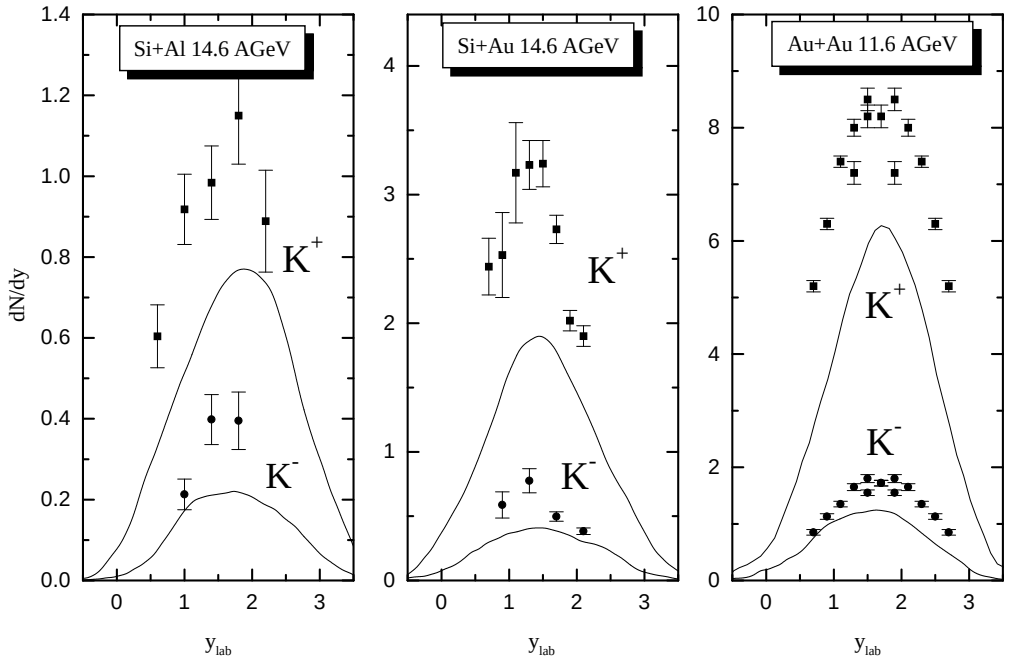

Figure 14: Inclusive K^+ and K^- rapidity spectra for Si + Al at 14.6 A·GeV (left), Si + Au at 14.6 A·GeV (middle) and Au + Au at 11.6 A·GeV (right) in comparison to the data from the E802 Collaboration [48] (for Si + Al and Si + Au) and from [58].

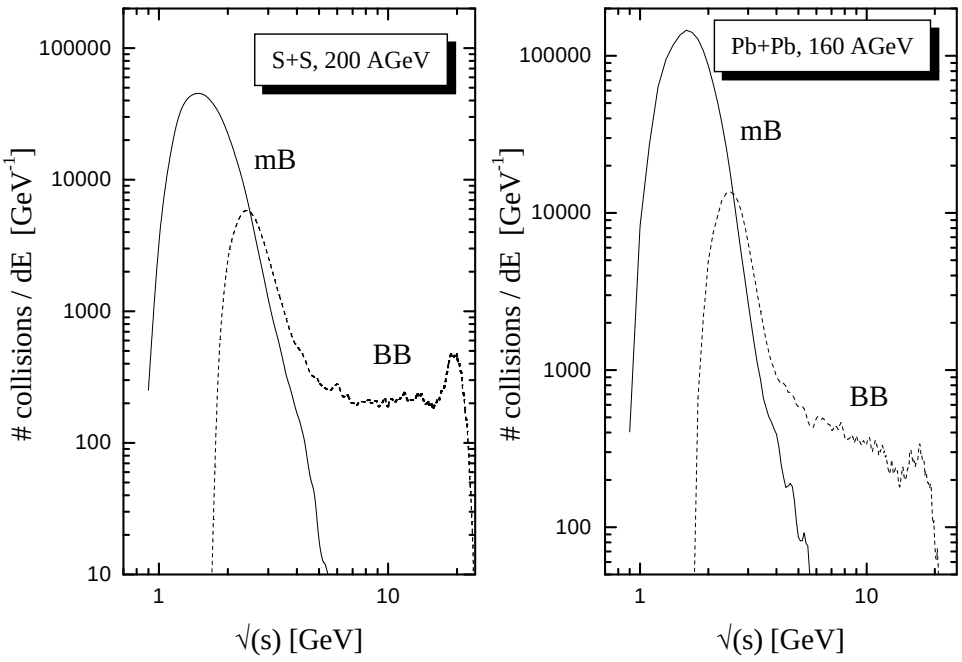

Figure 15: The number of baryon-baryon (dashed lines) and meson-baryon (solid lines) collisions as a function of the invariant collision energy $\sqrt{s}$ for central S + S collisions (l.h.s.) at 200 A·GeV and Pb + Pb collisions (r.h.s.) at 160 A·GeV.

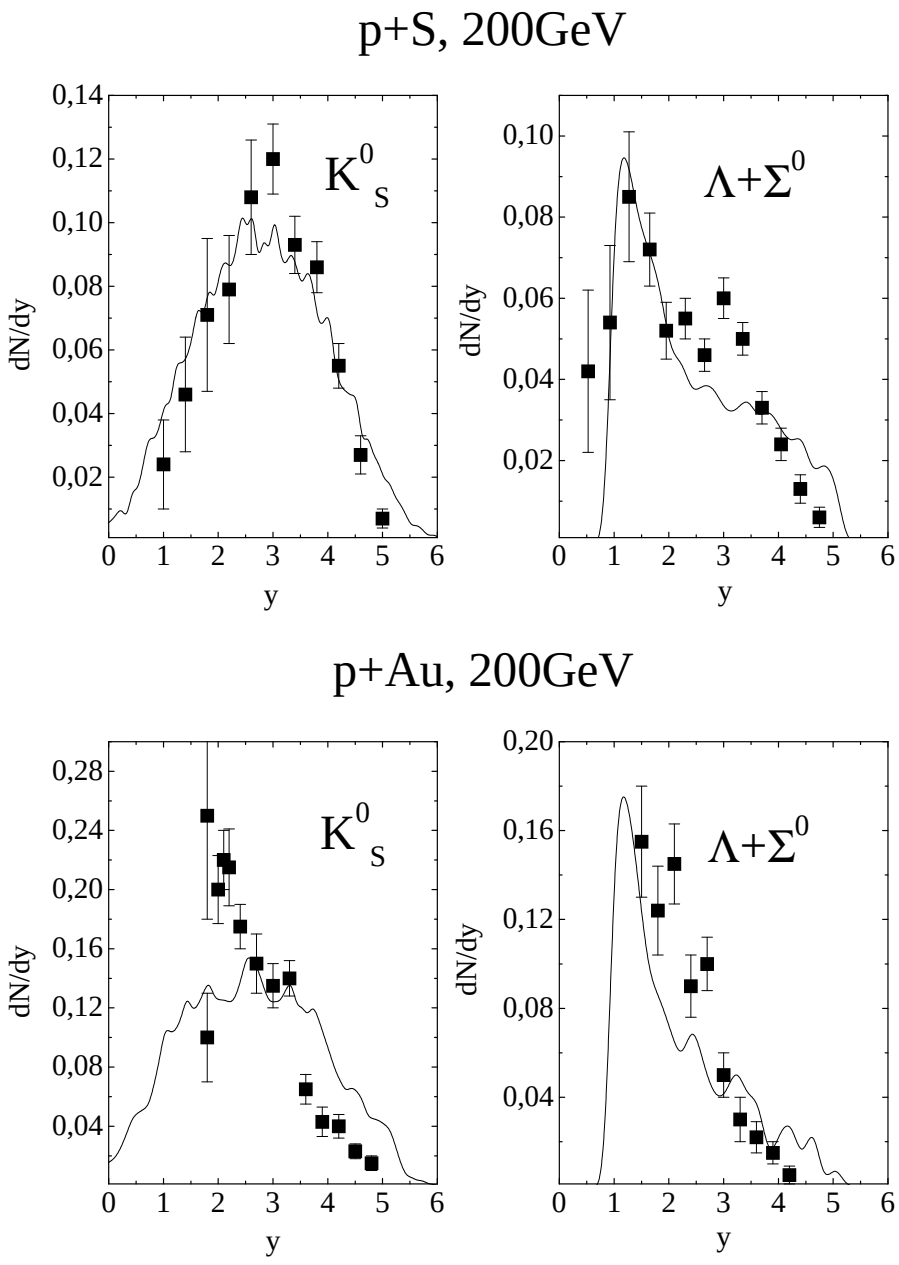

Figure 16: Comparison between the HSD calculations (lines) and data from NA35 [59] (squares) for the rapidity distribution of K^0_S (left) and hyperons $\Lambda + \Sigma^0$ (right) produced in p + S collisions (trigger condition: more than five charged particles in the NA35 streamer chamber) and minimum bias p + Au collisions at 200 GeV.

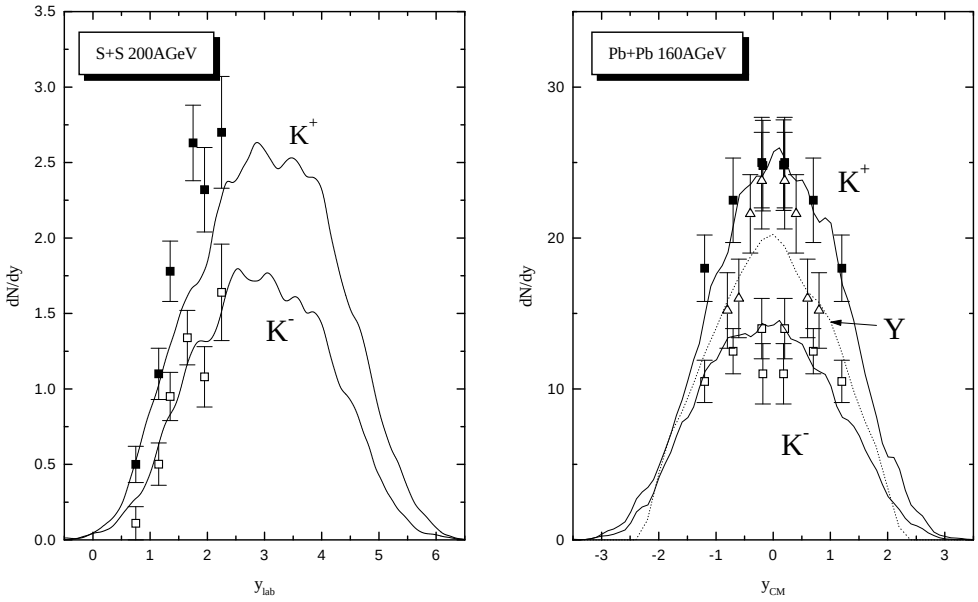

Figure 17: Inclusive K^+ and K^- rapidity spectra for central S + S collisions ($b \leq 1.5$ fm) at 200 A·GeV (left) and central Pb + Pb collisions ($b \leq 2.5$ fm) at 160 A·GeV (right) in comparison to the data from the NA35 Collaboration [51] and from the NA49 Collaboration [62]. The hyperon ($Y = \Lambda, \Sigma^0$) rapidity distribution for Pb + Pb is shown by the dotted line in comparison to the experimental data (open triangles) from [62].

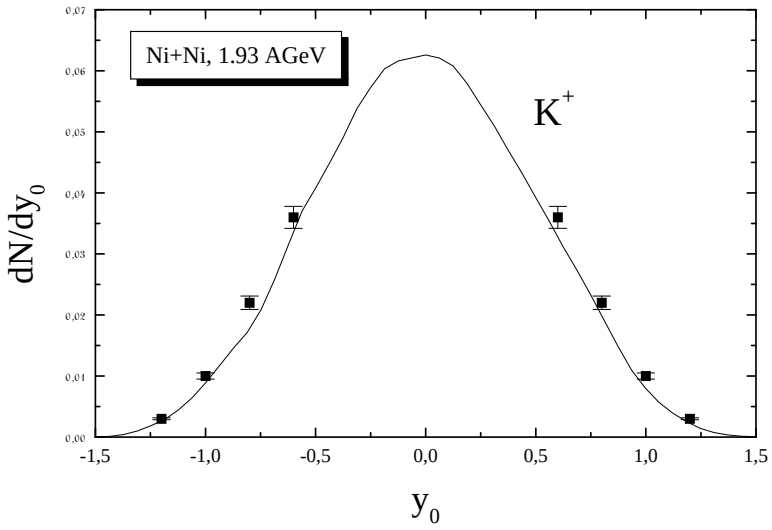

Figure 18: The calculated K^+ rapidity distribution for Ni+Ni collisions at 1.93 AGeV as a function of the normalized rapidity $y_0 = y_{cm}/y_{proj}$ in comparison with the FOPI data [64], which have been reflected around midrapidity.

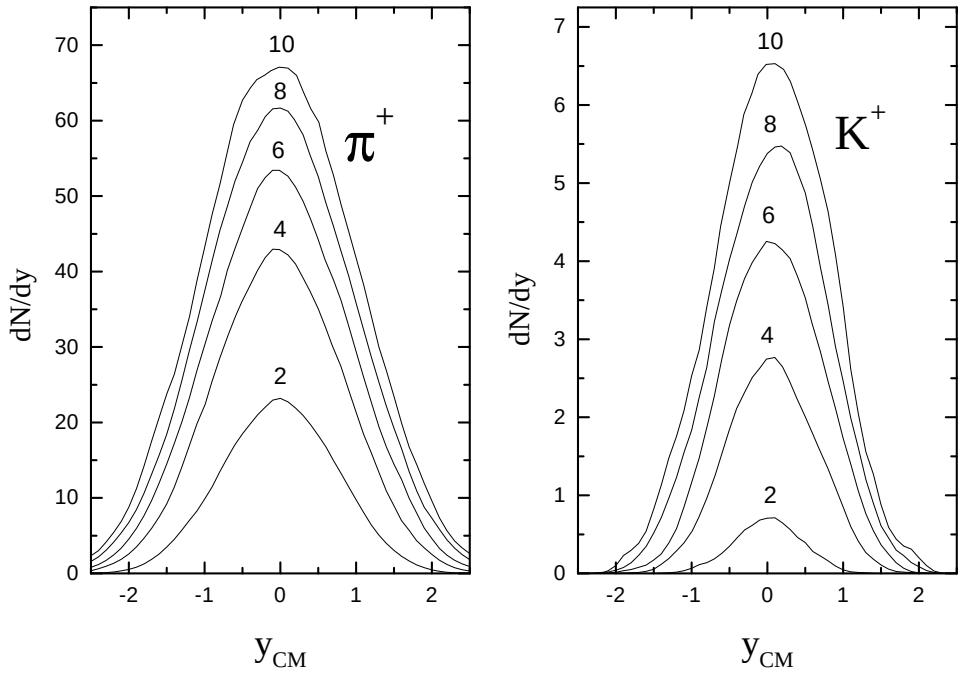

Figure 19: The calculated π^+ and K^+ rapidity distributions for central (b=2 fm) Au + Au collisions at 2,4,6,8 and 10 AGeV versus the rapidity in the cms.